https://doi.org/10.15407/ufm.23.02.296

V.Yu. DANILCHENKO*, Ye.M. DZEVIN, and O.M. SEMYRGA*****
G.V. Kurdyumov Institute for Metal Physics of the N.A.S. of Ukraine,
36 Academician Vernadsky Blvd.,
UA-03142 Kyiv, Ukraine
* danila@imp.kiev.ua, ** dzevin@i.ua, *** o_semyrga@ukr.net

PHASE AND STRUCTURAL TRANSFORMATIONS IN THE Fe-BASED ALLOYS UNDER THE COMBINED HIGH-ENERGY TREATMENT

Applying the x-ray, metallographic, and microdurometric methods, the phase composition and structural–stress state of the Fe-based alloys under the impact of electrospark treatment in combination with laser processing are studied and analysed. As shown, the structural–phase state of electrospark coating on the steel substrate is determined by several factors. They are the dissociation of WC carbide on the surface of alloying electrode on the W_2C and W components followed by their erosion, an interaction of erosion products with elements of the interelectrode medium (C, N, O), an interdiffusion of the coating elements and a steel substrate, and the ascending diffusion of C from the substrate near-surface layers. As revealed, the heterophase coating and near-surface layers of substrate possess a complex structural–stress state. As shown, the residual stresses in different phase components have been formed through different regularities: the tensile stresses in the TiC-based compound, while the compressed stresses in the W_2C, W, and Fe_α. The selective effect of laser heating of the coating on the stresses of different signs is revealed.

Keywords: electrospark treatment, laser treatment, residual stress, martensitic transformation, erosion, diffusion, mass transfer, carbide, nitride.

1. Introduction: Background of the Problem

Improving the physical and mechanical properties of metallic materials can be achieved by changing them in the near-surface layers in the desired direction or by applying the special coatings without changing the characteristics of the volume. The further development of these treat-

Citation: V.Yu. Danilchenko, Ye.M. Dzevin, and O.M. Semyrga, Phase and Structural Transformations in the Fe-Based Alloys under the Combined High-Energy Treatment, *Progress in Physics of Metals*, **23**, No. 2: 296–336 (2022)

ment methods and a significant increase in its efficiency is associated with a purposeful change in the chemical content and structural-phase state of the coatings and the surface layers of the substrate [1–4].

Creation of physical and technological fundamentals of intensive heat treatment by means of concentrated streams of energy can be carried out only with use of the fundamental regularities of formation of a phase and structurally-stressed state both own covering, and near-surface layers of a substrate. The interest is a study of the patterns of structure formation in materials that are in an extremely nonequilibrium state due to pulse loads, temperature gradients, high heating rates and subsequent cooling. Under these conditions, the processes are much more active than under conventional heat treatment and lead to the formation of a special heterophase and high-stressed state [4–6]. Peculiarities of structural transformations under nonequilibrium conditions of pulsed, for example, laser treatment (LT) or electrospark treatment (EST), have remained insufficiently studied. This situation complicates the definition of the relationship between the technological parameters of pulse treatment and the complex of physical and mechanical characteristics of the local areas of the processed alloys and still does not allow building a complete picture of the structure formation. This proved to be a brake on the further development of the basics of intensive heat treatment of metastable alloys.

With the combined surface treatment of alloys in the formation of the structural-phase state and a set of properties can take several factors with different physical nature. In some cases, energy of different types (mechanical, electrical, magnetic, *etc.*) can be supplied. This makes it possible to control the phenomena occurring in metals and alloys in the process of external influence — melting and evaporation, hydrodynamics of the molten layer, thermoplastic deformation, the formation of a magnetic domain structure and so on. It can be used to intensify the thermo-physical and chemical-thermal processes, dispersion of near-surface layers, control of formation or disintegration of supersaturated solid solutions, change of micro- and macrorelief of the surface. Intensification of interaction with the elements of a gaseous or liquid environment can lead to a significant absorption of these elements, such as nitrogen, carbon or oxygen from the atmosphere, and the formation of additional phase components of a strengthening nature. In some cases, obviously, one can expect a super-total effect from the simultaneous application of different physical influences, which will be expressed, in particular, in the formation of a structural-phase state significantly different from that achieved by consistent application of the same factors.

Non-stationary pulsed processes of heating and subsequent cooling of the material under conditions of temperature gradient in the area of electric discharge or laser beam and phase transformations with a sig-

nificant volumetric effect cause significant residual stresses. The nature of the distribution of stresses with depth, their magnitude and sign, along with the phase and structural state, effect on the formation of mechanical and, consequently, the exploitation properties of hardened details and products. However, the study of residual stresses after pulse treatment was carried out mostly in the main phase component of the coating or substrate, although the total structural stress state is the result of the interaction of stresses in all phase components. The study of the distribution of residual stresses in each of the phase components will allow building a complex picture of the stress state of the coating and substrate. This in turn will contribute to justification and correct choice of optimal modes of subsequent heat or laser treatment to relax the weakening tensile stresses and use an additional strengthening factor of the compressive stresses.

Control of the characteristics of phase transformations, particularly induced direct–reverse martensitic transformations of different types and redistribution of residual stresses, attracts additional opportunities for the formation of a set of properties in the process of intensive heat treatment [7–11].

Thus, the study of the fundamental regularities of formation of the phase and structural-stress state of coatings and near-surface layers of metastable alloys under conditions of nonequilibrium pulse treatment are actual.

The complex of physical and mechanical properties of the electrospark coated and near-surface hardened layers of the material is determined by their chemical content and structural-phase state. Repeated pulsed and thermal effects on the electrode material lead to complex mechanisms of electric erosion and mass transfer between the anode and cathode. Because of the erosion, the anode material enters in the discharge channel and the interelectrode gap in the form of particles in the vapour, liquid droplets and solid phases. These particles bombard the substrate and participate in the formation of the electrospark coating (ESC), doping and strengthening of its near-surface layers. Such an intense effect can significantly change the distribution of chemical elements in the coating and in the hardened base layer, as well as change their phase content and structural state [3, 4, 12, 13].

The processes of interaction with the elements of the interelectrode gas or liquid environment, crystallization, diffusion, phase transformations that take place during the formation of the coating, determine a high degree of non-equilibrium and heterogeneity of the formed structure. The choice of the content of the alloying electrode and the optimal modes of ESC can be made based on the use of fundamental regularities of formation of the phase state in the materials of the electrode and the substrate. However, such regularities in the literature are insufficiently

studied, which does not allow to formulate criteria for selecting the chemical and phase content of hard alloys for alloying electrodes and purposefully control the complex of physical and mechanical properties of the ESC. In this regard, it is important to study the phase content and distribution of residual stresses in hard alloys ESC and hardened near-surface layers of steel substrate.

This article reviews the experimental works of the G.V. Kurdyumov Institute for Metal Physics of the National Academy of Sciences of Ukraine on the study of fundamental regularities of formation of the phase and structural-stressed state of the iron-based alloys under the influence of EST and LT.

2. Materials and Methods

The EST of the steel substrate of Fe–0.75% C–0.2% Mn–0.19% Si–0.25% Ni (wt.%) was carried out in the air at the 'Elitron' equipment. The magnitude of the application current was varied in the range of 0.5–2.8 A. The coating time was from 1 to 5 minutes. To prevent the electrode from sticking to the sample, a mode with electrode vibration with a frequency of 50 Hz was used. ESC was applied using the electrode alloy. The size of the fractions of the electrode material did not exceed 100 μm. Phase content of the electrode alloy — 15% TiC and 6% Co; the residual — WC (wt.%).

Microstructural studies of the ESC were performed on the surface and in the cross section of the samples. Transverse sections were made on an electrospark machine in transformer oil, followed by mechanical grinding and chemical etching of the section surface in a concentrated solution of acids (25% HNO_3, 75% HCl).

LT was performed on the Quant-18M equipment (pulsed solid-state laser on neodymium glass, radiation wavelength 1.06 μm, pulse duration 8 ms, pulse repetition frequency 0.5–5.0 Hz) with energy in the pulse from 0.1 to 2.0 J/mm^2. The output energy was monitored with a calorimetric IST-1N meter. The surface of the samples was treated with single pulses with a follow-up period 0.5–1.0 s with mutual overlap of laser spots by 30–40%. LT was carried out in the mode of laser heating (0.1–0.45 J/mm^2), pre-melting (0.5–0.7 J/mm^2), and melting (0.8–2.0 J/mm^2). In the melting mode, a welding nozzle was used, which provided the possibility of focusing the laser beam. For uniformity of laser heating, the coordinate table with micrometric giving was used. LT of TiC powder was performed in air atmosphere with a defocused laser beam with a spot diameter of 5 mm and an energy density of 1.4 J/mm^2.

Metallographic studies of ESC performed using MIM-7 optical microscope at a magnification of 50 to 800. The surface of the samples mechanically polished with abrasive paper and on the dress using a po-

lishing paste based on chromium oxide. The microstructure of ESC was detected by chemical etching in 20% alcohol solution of 25% HNO_3 + + 75% HCl and in 20% alcohol solution of hydrogen peroxide after heating the sample to a temperature of 100 °C in boiling water. To better wet the sections, a small amount of surfactant was added to the etching solution. The microhardness of the ESC and the substrate material was measured with a PMT-3 microhardness tester. As an indenter, it is used a diamond pyramid with a square base and an angle at the apex of 136°. Measurements were performed at loads of 20, 50, and 100 g. The magnitude of the load depended on the thickness of zones, formed during EST, and on their microhardness.

The study of the microstructures of the ESC surface in the initial stages of its formation was performed using a scanning microscope 'Philips'. The distribution of chemical elements in different zones of the ESC and its subsequent LT was studied using an x-ray probe in a scanning microscope.

The distribution of elements along the ESC depth was studied by the x-ray spectral method on the 'Jeol Superprobe' equipment with an acceleration voltage of 25 KV at a magnification of 3000. Images of the coating were obtained in K_α and L_α radiation, as well as in secondary electrons. A differential magnetometer assembled based on the BU-3 equipment was used to measure the critical points of direct and reverse martensitic transformation. Cylindrical samples with a diameter of 3 mm and a length of 20 mm were used. The accuracy of measuring the amount of martensitic phase was 0.5%.

X-ray studies of ESC were performed on an automated diffractometer DRON-3 in iron, cobalt and copper radiation using a graphite monochromator. The amount of phase components was measured by the intensity of diffraction reflexes taking into account the repeatability factor of the corresponding crystallographic planes of the lattices of phase components and the absorption coefficients of x-rays by different elements according to the formula [14]: $M_i = I_i \mu_i (p_i \Sigma_i (I_i \mu_i / p_i))^{-1} \cdot 100\%$. Here, M_i is the mass fraction of the i-th phase, I_i is the intensity of the corresponding reflex, p_i is the repeatability factor of the crystallographic plane, and absorption coefficient $\mu_i = N\tau_i Z_i / \rho_i A_i$ [15]. In the last relation, Z_i is a serial number of the i-th element in the periodic table, ρ_i is a density of the i-th element, A_i is an atomic mass of the i-th element, N is the Avogadro's number, τ_i is an atomic absorption coefficient of the i-th element.

For carbides and nitrides of the Me_xC or Me_xN type, the absorption coefficient defined as [16] $\mu_{Me_xC(N)} = (x\mu_{Me} + \mu_{C(N)})/x$, where μ_{Me} is an absorption coefficient of the metal component of carbide (nitride), $\mu_{C(N)}$ is the carbon (nitrogen) absorption coefficient, and x is an amount of metal atoms in the carbide (nitride). The accuracy of measuring the amount of phase components was 5%.

Studies of the regularities of residual stress formation were performed by the non-destructive x-ray method $\sin^2\psi$. Measurements were performed on individual reflexes of each phase component with a sequential inclination of the sample by 5°, 10°, 15°, 25°, and 30° from the normal reflection position of the diffracted beam. The surface of the ESC or laser path was examined with a narrow diffracted beam. The projection of the primary beam in the area of formation of the diffraction reflex was significantly smaller than the area of laser treatment. The accuracy of stress measurement was equal to ±10 MPa.

3. Results, Analyses, Discussions

3.1. Regularities of the Formation of Phase Content and Structural-Stressed State of the Steel Substrate and Coating

Microstructure studies have shown uneven of thickness and discontinuity of ESC (Fig. 1) [17]. The phase content of the electrode and coating from it differed significantly. The change in the phase content of the electrode material in the process of its erosion and subsequent deposition on the substrate has been reported in the literature: see Refs. [8–10] and references therein.

The diffraction pattern of the coating did not reveal reflections from the main structural component of the electrode — WC carbide. From the plasticizing addition as Co, only traces of reflexes were recorded. Additionally, reflexes from the hexagonal lattice of W_2C carbide and b.c.c. of pure tungsten lattice were revealed. Weak reflexes from high-speed steel carbide Fe_3W_3C and traces of oxides were also detected. The most intensive x-ray reflexes of the coating surface were TiC reflexes. The diffraction pattern also contained reflexes from the f.c.c. lattice of austenite (γ-phase), the amount of which was much higher than in the initial steel substrate before ESC. As previously found, the formation of carbon γ-solid solution is characteristic of EST of iron and cobalt alloys [8]. In addition, the reflections from the b.c.c.

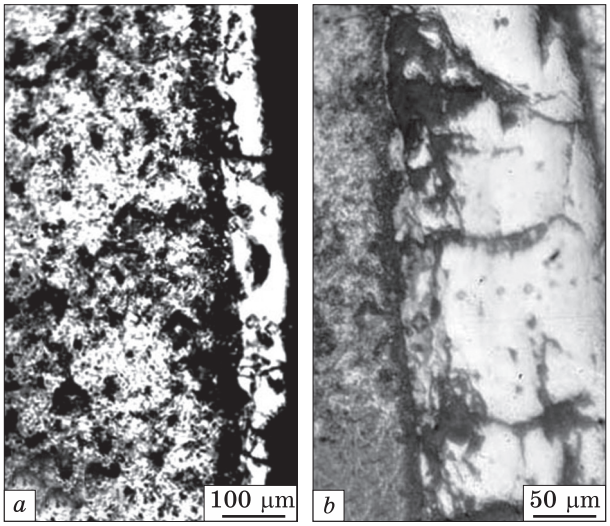

Fig. 1. Microstructure of different regions of the ESC [17]

Table 1. **Interplanar distances and relative intensity of reflexes of phase components of ESC on steel substrate (parameters: 1.8 A, 5 min) [22]**

D/n_{exp}	I_{exp}	Fe_α			Fe_γ			TiC		
		hkl	*D/n*	*I*	*hkl*	*D/n*	*I*	*hkl*	*D/n*	*I*
2.48	0.8							111	2.49	0.75
2.261	0.05									
2.222	0.3									
2.142	1							200	2.15	1
2.11	0.4				111	2.07	1			
2.037	0.4	110	2.01	1						
1.818	0.1				200	1.80	0.5			
1.580	0.1									
1.540	0.1									
1.52	0.4							220	1.52	0.5
1.426	0.1	200	1.428	0.2						
1.290	0.4				220	1.26	0.3	311	1.300	0.25
1.260	0.05							222	1.245	0.1
1.171	0.1	211	1.166	0.4						
1.071	0.15				311	1.081	0.3	400	1.079	0.03
1.020	0.05	220	1.010	0.1	222	1.018	0.04			
0.983	0.05							331	0.990	0.05
0.964	0.05							420	0.965	0.1

D/n_{exp}	I_{exp}	W			W_2C			Fe_3W_3C		
		hkl	*D/n*	*I*	*hkl*	*D/n*	*I*	*hkl*	*D/n*	*I*
2.48	0.8							331	2.52	0.7
2.261	0.05				101	2.27	1	422	2.249	0.9
2.222	0.3	110	2.23	1						
2.142	1							511	2.122	1
2.11	0.4									
2.037	0.4									
1.818	0.1									
1.580	0.1	200	1.58	0.3						
1.540	0.1							551	1.545	0.7
1.52	0.4				110	1.50	0.3			
1.426	0.1							553	1.440	0.7
1.290	0.4	211	1.290	0.7	103	1.349	0.6			
1.260	0.05				112	1.270	0.6			
1.171	0.1	220	1.117	0.1						
1.071	0.15									
1.020	0.05	310	1.000	0.2	203	1.002	0.6			
0.983	0.05									
0.964	0.05									

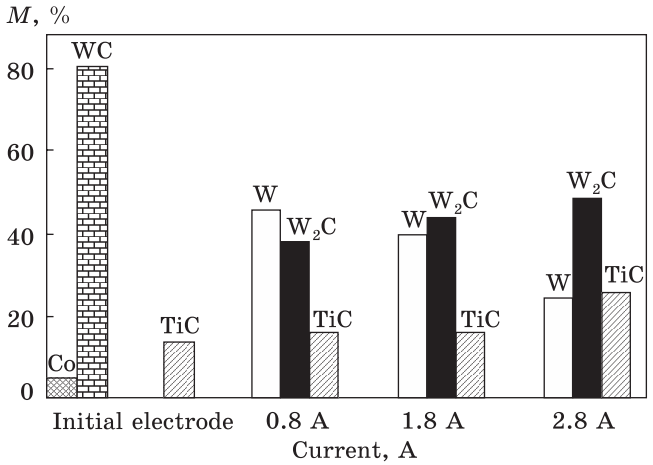

Fig. 2. Change of phase components in the ESC depending on the magnitude of current for 2 min of treatment [17]

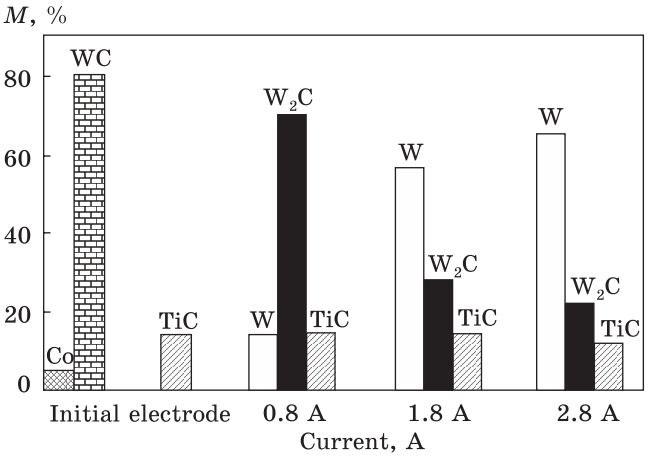

Fig. 3. The same as in the previous figure, but for coating time of 5 min [17]

of the α-phase lattice of steel substrate were recorded. The results of the study of phase content of the coating are shown in Table 1.

The possibility of observing reflexes from γ- and α-phases belonging to the steel substrate is associated with small thickness and discontinuity of 65–70% ESC [10]. The thickness of the ESC was comparable to the depth of penetration of the x-ray beam of an iron anode. Due to the difference in the erosion ability of the electrode materials, the phase components of the coating were distributed differently at the depth at which the corresponding diffraction reflexes were formed. For this reason, in Figs. 2 and 3 show the content of phase components without taking into account their distribution along the depth of penetration of the primary x-ray beam [17].

The phase content of the coating significantly depended on the EST mode. With increasing current and application time, the content of W

increased (Figs. 2 and 3). The reason for this may be that under the action of high temperatures of the spark discharge the carbide WC of electrode dissociated into carbide W_2C and pure tungsten with the release of atomic carbon.

The energy of WC formation dissociation products, as well as other possible compounds that can be formed during high-energy treatment of materials of the electrode alloy, is given in Table 2.

The dissociation reaction took place already on the surface of the doping electrode. Indeed, the formation of tungsten under the influence of an electric spark was observed by x-ray method on the surface of the electrode alloy. The particles trapped in the interelectrode gap because of the brittle fracture of the WC carbide were apparently further dissociated, and thus the initial WC carbide phase was no longer detected in the ESC. Pure tungsten accumulated on the electrode because its erosion resistance was higher than W_2C, TiC, and Co. Because of this, we can assume that under intensive modes the dissociation is more active at the electrode itself. Measurements of the phase content of the coat-

Table 2. **Formation energy for possible compounds as a result of EST of electrode alloy, where '–' and '+' — released and absorption energies [22]**

Compound	Formation energy, kcal/mole	Temperature interval, K	Literature
WC	–9.1 –5.4	571–2273 571–3273	[19]
W_2N	–17.2		[21]
W_2C	+11.7	571	[20]
WO_3	–200		[22]
WO_2	–134.5		[22]
Co_2C	–0.4		[19]
Co_3C	+4.0		[20]
TiC	–43.75 –44.6	571–1428 1428–2273	[20]
TiN	–80.3 –80.9	571–1428 1428–2046	[20]
TiO	–123.9	571	[23]
TiO_2	–225.6	571	
Fe_4N	–0.2	571–1223	[20]
Fe_3C	+6.2 +6.4 +2.5	571–736 736–1115 1388–1805	[21]
FeO	–63.2		[21]
Fe_3O_4	–266.9		[21]
Fe_2O_3	–196.3		[21]

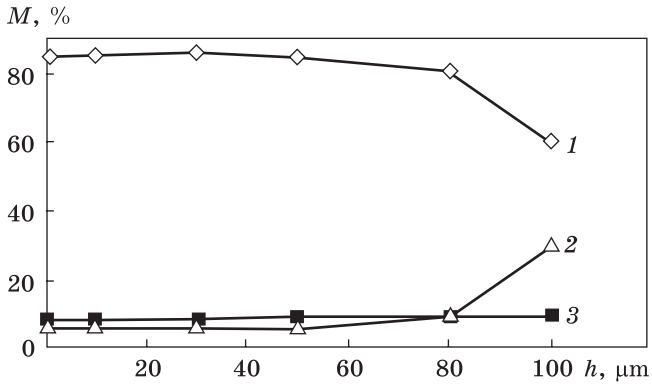

Fig. 4. Amount of the phase components *vs.* the depth of the ESC, where *1* — W, *2* — W_2C, *3* — TiC [18]

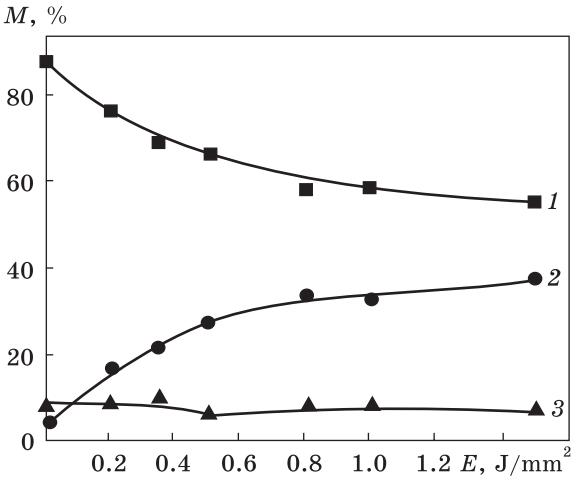

Fig. 5. Amount of phase components of the ESC *vs.* the energy density of laser beam, where *1* — W, *2* — W_2C, *3* — TiC [18]

ing, performed using mechanical grinding, showed an increase in the content of W_2C by depth of coating (Fig. 4), which confirms the conclusion about the accumulation of W at the electrode and greater erosion ability of W_2C [18].

The Co reflexes there were no observed during the x-ray studying of the ESC surface. It means that Co transferred from the electrode to the steel substrate is able to dissolve almost completely in Fe because of the interaction of components in the liquid phase. There is a possibility of formation of unlimited solid solutions and dissolution in the W released because of the dissociation of the initial WC carbide.

This experimental fact has shown the feasibility of using in the alloying electrode as a plasticizing component of such metals, which in the process of forming the coating at high temperatures dissolve in γ-iron and therefore do not create additional residual stresses. These requirements are met, *e.g.*, by metals such as Ni, Co, and Cr.

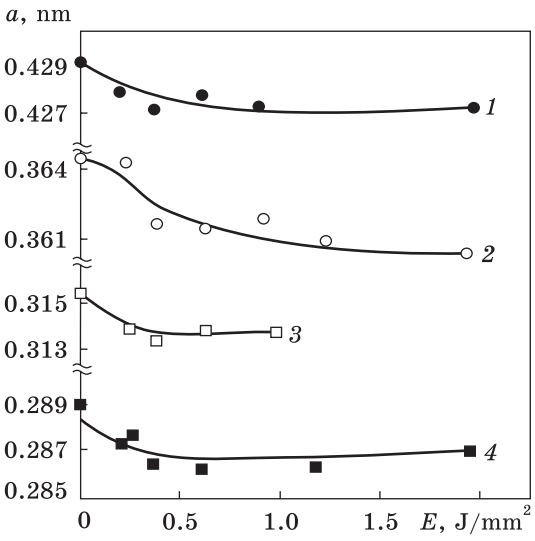

Fig. 6. Lattice parameter of the phase components of the ESC *vs.* the energy density of laser beam, where *1* — TiC, *2* — Fe_γ, *3* — W, *4* — Fe_α [18]

LT lead to change of the properties of ESC [24, 25]. Therefore, it was of interest to study the effect of laser heating on the structural-phase content of ESC. It turned out that the amount of TiC did not change when heated with the energy density of the laser beam to 1.6 J/mm^2, and the amount of W_2C increased significantly (up to 20%) due to a corresponding decrease in the amount of pure tungsten (Fig. 5). The reason for this was the secondary carbonization of tungsten under the condition of the initial diffusion of carbon from the substrate under the action of tensile residual stresses in the near-surface layers of the coating. Therefore, laser heating of ESC allows increasing the amount of tungsten carbide W_2C, which is an additional strengthening factor.

When the energy density increased above 1.6 J/mm^2, convective mixing of the phase components of the coating with the substrate material took place, because of which the phase content corresponded to another phase diagram.

LT of the coating caused a decrease in the parameter of the crystal lattice of the phase components. In this case, carbon burned out from α- and γ-solid solutions of iron (Fig. 6, curves *2* and *4*) [18]. After the EST, the lattice parameter of the α-Fe was greater than the parameter of pure Fe, and the asymmetry of the $\{200\}_\alpha$ reflex indicated a small tetragonality of the α-phase. This meant that due to the rapid cooling after EST in the near-surface layer of the substrate, the martensite of quenching formed, which disintegrated after subsequent laser heating. The decrease in the TiC lattice parameter indicated the formation of TiCN solution (Fig. 6, curve *1*). The change in the value of the W lattice parameter is because the EST formed a solution of W–Co–Fe, unstable

under conditions of intense laser heating (Fig. 6, curve *3*). After heating with an energy density higher than 1.0 J/mm^2 W partially dissolved in Fe_γ and passed into the carbide phase, because of which the reflexes from its lattice were no longer fixed.

In a more detailed phase analysis, it should be borne in mind that all titanium oxides have higher activation energy than titanium nitride. TiN is able to react with oxygen to form oxides of titanium and free nitrogen [26]. This phenomenon can occur during laser heating of the formed ESC.

3.2. Crystal Structure of TiC-Based Compound Synthesized by the EST

The lattice parameter a_{TiC}, determined from the diffraction pattern of the initial electrode, was equal to 0.429 nm, *i.e.* was less than the parameter of this phase in the ESC. For example, in the coating mode I = 0.8 A, 2 min, the parameter a_{TiC} was equal to 0.4254 nm, and at I = 2.8 A, 2 min, the a_{TiC} parameter increased to 0.4270 nm. Mechanical grinding and chemical etching showed that the a_{TiC} parameter decreased with the depth of coating (Fig. 7) [27]. There are two reasons for the decrease in a_{TiC} on the surface of the coating and its depth.

The first possible reason for the decrease in a_{TiC} in the ESC is related to the nitriding of the TiC compound in the discharge channel during the mass transfer between the electrodes. In the discharge channel, atmospheric molecular nitrogen decomposed into atomic, highly reactive. It is obvious that under certain conditions nitrogen plasma can be formed with nitrogen ions with increased reactivity. Therefore, free titanium, as a product of partial dissociation of TiC, can react with nitrogen to form titanium nitride TiN. In addition, nitrogen at high temperatures and pressures in the discharge channel is able to interact with TiC, partially replacing carbon with the formation of solid solutions of TiCN in the ESC. This possibility appears in connection with the thermodynamic advantage of the formation of TiN compared to TiC (the heat of formation of TiC and TiN at different temperatures is –43.75, –44.6; and –80.3, –80.9 kcal/mole, respectively, as listed in Table 2).

TiC and TiN compounds form a continuous series of solid solutions and the change in the crystal lattice parameter practically corresponds to Vegard's rule [26]. In Figure 8, it is shown a linear characteristic of the parameter a depending on the

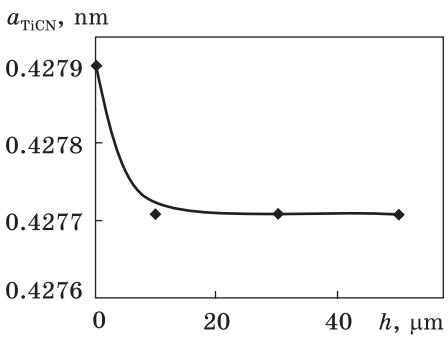

Fig. 7. Lattice parameter a_{TiCN} as a function of the coating depth [27]

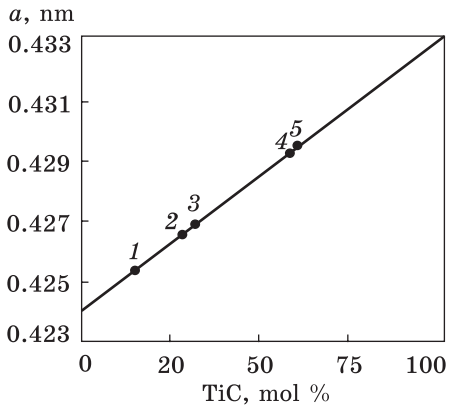

Fig. 8. Lattice parameter of the TiC-based solid solution for different modes (regimes) of the ESC treatment: *1* — 0.8 A, 2 min; *2* — 1.8 A, 2 min; *3* — 2.8 A, 2 min; *4* — 0.8 A, 5 min; *5* — 1.8 A, 5 min [28]

ratio of TiC:TiN [28]. It is convenient to plot the experimental values of a_{TiC} on this line. This allows us to calculate the proportion of solid solution of TiN formed during the mass transfer of TiC through the interelectrode gap. It is seen that under different coating modes, the ratio of TiC–TiN varied. For example, in mode I = 0.8 A, 5 min the TiN fraction was 40% (Fig. 8). The amount of carbon or nitrogen in TiCN carbonitride can be determined from the magnitude of the decrease in a_{TiC}. It is known from the literature that the hardness of carbonitride is also an additive value and is the sum of the hardness of the double systems TiS and TiN [29].

During laser heating ESC, the parameter a_{TiC} also changed. The increase in the energy density of the laser beam led to a decrease in a_{TiC}, which is evidence of an increase in the nitrogen content in the synthesized compound TiCN. From the change in the value of a_{TiC}, it was calculated that at laser heating with an energy density of up to 1.2 J/mm^2, the TiN content in the ESC was 18%. By means of spectral analysis of plasma in the interelectrode gap in combination with the sweep of the spectrum over time, the presence in the working spectrum of elements of the environment (N and O) was shown. X-ray studies of the alloyed layer of the steel substrate confirmed the presence of iron and titanium nitrides in this layer [8]. The x-ray spectral method showed that when doping steels with niobium carbide in the near-surface layers was recorded up to 0.72 wt.% of nitrogen, and when doping with chromium carbide the nitrogen content reached 2.5 wt.% due to the high ability of chromium released by dissociation to absorb nitrogen [30]. In our work, a sign of the presence of TiN nitride in the ESC was the appearance of a characteristic golden colour of the coating surface at certain modes of electric spark. It was previously shown that the crystals of titanium carbonitride isolated from steel changed colour from yellow to grey depending on the ratio of TiC–TiN [29].

The formation of nitrides in the coating can be useful because, compared to carbides, they have a low friction coefficient on alloys based on iron and high abrasion resistance [8]. Another reason for the reduction of a_{TiC} in ESC is the defectiveness of the TiC lattice on carbon. TiC_x carbide exists in a sufficiently wide interval of homogenic solid solutions

($1 > x > 0.5$). At the same time, the metal lattice is always complete, and the defection of carbon sublattice in significant limits can change during the technological process of making and compacting of titanium carbide powders, as well as a result of the subsequent impact of electric spark on the surface of both an anode and cathode. As the defection on carbon increased, the a_{TiC} parameter decreased. The parameter of the TiC carbide lattice according to the limits of its homogeneity varied within 0.4260–0.4320 nm. In the output electrode, this parameter was slightly smaller (0.4310 nm) from the parameter for the stoichiometric content of the TiC. This indicated a certain defect of the carbon lattice. Similarly, the TiN compound may also have a defective nitrogen sublattice and, as a result, the a_{TiN} parameter may be variable. The a_{TiN} parameter varied linearly from 0.4234 nm for the nitride of the stoichiometric TiN content to 0.4213 nm for the content at the lower limit of homogeneity ($TiN_{0.42}$). It should be noted that the microhardness of TiC and TiN varied linearly depending on the non-metal content in the region of phase homogeneity [29]. Therefore, it can be assumed that the decrease in a_{TiC} observed in this work is due to the partial dissociation of TiC in the electric discharge channel. Because of dissociation, the carbide lost carbon, and the pure titanium released entered the steel substrate in a liquid-droplet or vapour phase that adhered well to the substrate, and as a result interacted with it. In Ref. [19], the x-ray diffraction analysis of TiC_x erosion products showed that with increasing carbon vacancies in the ESC carbide lattices, the content of free titanium diffused into the steel substrate and bound the dissolved carbon to the carbide phase. This led to increased carbon content in the surface layer of the steel substrate and the depletion by carbon of thermal influenced zone.

In the case of partial dissociation of TiC at the doping electrode and an increase in the defect of carbon carbide erosion of titanium carbide, the proportion of fine particles in the erosion products and the total weight addition of the steel cathode decreased in accordance with the weakening of the covalent Ti–C bond and the strengthening of Ti–Ti bonds [19]. Increasing the erosion resistance of titanium carbide in the set of $TiC_{1.0}$–$TiC_{0.6}$ leads to the fact that the dissociation of TiC directly on the anode surface is technologically undesirable. It is obvious that the dissociation of TiC carbide took place during evaporation, and in the discharge channel, the dissociation process further developed.

There is reason to believe that solid carbon and nitrogen solutions were formed in the ESC due to the implementation of both mechanisms of nitrogen uptake both in the discharge channel and because of bombardment of the electrode surface. Their contribution to the formation of a solid solution of TiCN is obviously additive. The fact of reducing the carbide lattice parameter by the depth of the coating suggests that the processes of dissociation of titanium carbide and its nitriding in the

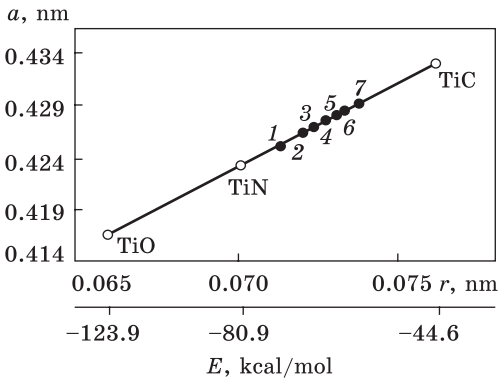

Fig. 9. Lattice parameter *a* of the Ti compounds *vs.* the radius *r* of non-metal, where points *1*–*7* — the parameter values at the different modes of spark and laser treatment [28]

discharge channel are more active in the initial stages of coating formation.

Figure 9 shows the linear dependence of the f.c.c. lattice parameter of carbide, nitride and titanium oxide on the radius of non-metal atoms [28]. Comparison of the formation energy of compounds shows that in the process of EST or LT titanium carbide may be energetically beneficial the formation of TiN or TiO. At EST in air, there is an intensive absorption of oxygen and nitrogen by titanium with formation of solid solutions. The rate of oxygen uptake was much higher than that of nitrogen [31–33]. The experimental values of the parameter fell between the values for TiC and TiN. It can be seen that the formation of TiN and TiO compounds by pulse treatment significantly reduced the integral parameter of the crystal lattice of the synthesized solid solution. Thus, high-energy treatment of TiC formed a complex compound comprising isomorphic f.c.c. components and its chemical content can be conventionally defined as TiCNO. The complex TiCNO carbonitride oxide formed during EST or LT of TiC carbide will be hereinafter referred to as a TiC-based compound for simplicity.

In the study of the phase content, a noticeable deviation of the relative intensity of the reflexes from the theoretical one was observed, which testified to a certain texturing of the coating. Comparison of the relative intensity of TiC reflexes showed that a texture close to the growth texture was formed during the formation of ESC. The ratio of the reflex intensity $(I_{111}/I_{200})_{TiC}$ varied from 1.1 to 1.9, respectively, at the magnitude of the electric current of treatment of 0.8–2.8 A (theoretical value for the f.c.c. lattice is of 0.75). This meant that crystallites of orientation ⟨111⟩ were formed mainly in the coating. The ratio of reflexes $I_{(220)}/I_{(200)}$ varied from 0.43 to 0.63 in different modes (Table 3), which differed little from the theoretical one — 0.5. The same nature of the texture for the ratio of reflexes $I_{(200)}/I_{(111)}$ was observed for austenitic lattices.

The mass transfer of TiC from the doping electrode in the EST process was carried out in the solid phase, but the carbide particles were subjected to surface melting, and as a result, a certain phase texture was formed.

The texture of the austenitic phase was formed under conditions of melting of the substrate. For the components of coating with the b.c.c. lattice, texturing was formed in the direction which perpendicular to the plane (110), due to more intensive heat dissipation. With increasing current and treatment time, the texture continued to develop in these directions. Such strong degeneration of the tungsten texture is the cause of erosion mainly in the liquid phase. For the W_2C component, the reflex ratio $I_{(103)}/I_{(101)}$ was recorded, which differed little from the theoretical one.

Laser heating had almost no effect on the change in texture obtained after EST (Table 4). However, already in the process of transition through the ESC melting threshold, the intensity of $(200)_\gamma$ and $(200)_{TiC}$ reflexes increased in 5–7 times similarly to the same changes in the formation of the austenitic phase texture by laser melting of construction steel [9, 32], and for all components observed smaller deviations from the theoretical value.

Table 3. **The relative intensity of x-ray reflexes of the phase components of ESC for different EST modes [22]**

Application mode	TiC		Fe_α	Fe_γ	W	W_2C
	$I_{(111)}/I_{(200)}$ (0.75)	$I_{(220)}/I_{(200)}$ (0.5)	$I_{(200)}/I_{(110)}$ (0.15)	$I_{(200)}/I_{(110)}$ (0.5)	$I_{(200)}/I_{(111)}$ (0.3)	$I_{(103)}/I_{(101)}$ (0.7)
0.8 A, 2 min	1.10	—	0.14	—	0.6	—
1.8 A, 2 min	1.11	—	0.25	—	0.9	—
2.8 A, 2 min	1.91	0.43	0.49	1.27	0.54	—
0.8 A, 5 min	1.01	0.63	0.49	—	0.33	—
1.8 A, 5 min	1.27	0.57	0.32	1.75	0.33	0.6
2.8 A, 5 min	1.37	0.48	0.32	—	0.52	0.75

Table 4. **The relative intensity of x-ray reflexes of the phase components under the laser heating ESC (at 1.8 A, 5 min) [22]**

The energy density of the laser beam, J/mm^2	TiC		Fe_α	Fe_γ	W	W_2C
	$I_{(111)}/I_{(200)}$	$I_{(220)}/I_{(200)}$	$I_{(200)}/I_{(110)}$	$I_{(200)}/I_{(110)}$	$I_{(200)}/I_{(111)}$	$I_{(103)}/I_{(101)}$
Initial sample	1.27	0.57	0.32	0.33	0.75	0.18
0.2	1.49	0.59	0.51	—	—	—
0.25	1.22	0.52	0.45	—	—	—
0.3	1.39	0.6	0.61	—	0.37	0.16
Melting						
0.35	0.84	0.32	0.54	1.17	0.56	—
0.6	1	0.57	0.56	0.89	0.4	—
0.8	1.1	0.27	0.37	1.38	0.38	0.1
1	—	—	0.18	0.47	—	—
1.5	—	—	0.2	0.5	—	—

Subsequent LT for W_2C showed an increase in the number of crystallites with [101] orientation. At the time of a significant increase in the intensity of these reflexes, we can offer a method for determining the moment of laser melting ESC similar to steel melting [32], which may be useful in developing of technological modes of combined EST and LT of the steel products.

3.3. Effect of LT on the Structural-Phase State of Initial Materials and ESC

EST and LT are intensive methods of treatment of the metals and alloys that can significantly change the degree of the structure imperfection. In this regard, we investigated the change in the physical half-width of the β reflexes in different phase components of the ESC and the reinforced near-surface layer of the steel substrate, and estimated the density of dislocations ρ in these components. The β value under the influence of laser heating varied differently for different phase components (Fig. 10) [34]. The ρ value was calculated from the physical half-width of the corresponding diffraction reflexes according to [35, 36].

In the coating components TiC, W_2C and W after EST, the ρ value was $2.4 \cdot 10^{10}$ cm^{-2}, $3.4 \cdot 10^{10}$ cm^{-2} and $1.7 \cdot 10^{10}$ cm^{-2}, respectively. The density of dislocations ρ in the doped layer of the substrate was close. For the components Fe_α and Fe_γ, the ρ value was $3 \cdot 10^{10}$ cm^{-2} and $2.5 \cdot 10^{10}$ cm^{-2}. Figure 11 shows that the half-width of the reflex $(211)_\alpha$ was maximal on the surface of the substrate [17]. The increased density of dislocations was caused by thermomechanical shock loading from periodic pulse discharges and the reactive action of the plasma jet. The shock mechanical wave, which arose at the initial stage of the discharge, led to the formation of dislocations in the local areas of the coating and the doped layer of the substrate, as well as the development of plastic deformation. In addition, under the influence of high local stresses close to the yield strength of the material, dislocations can occur under the action of only these stresses [37, 38]. Therefore, the formation of dislocations can occur after the completion of EST under the action of residual stresses. Obviously, additional dislocations can occur under the action of both tensile and compressive stresses.

The density of dislocations formed as a result of EST was close to the density that occurs in iron-based alloys due to high-degree deformation or phase hardening from the γ–α–γ martensitic transformations [8, 9].

As known, the amount of alloying element transferred to the near-surface layer of metal under the pulse loadings can be determined through the density of dislocations in this layer [39]. In [40] found the surface saturation of steel by carbon from a special technological environment under the condition of dislocation accumulation in the process

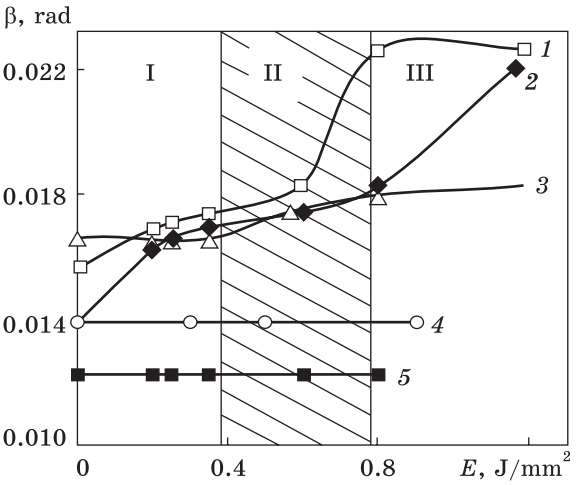

Fig. 10. Physical half-width β (in different phase components) *vs.* the energy density of laser beam: *1* — $(110)_{\alpha}$, *2* — $(220)_{TiC}$, *3* — $(200)_{\gamma}$, *4* — $(103)_{W2C}$, *5* — $(110)_{W}$; *I* — heating without melting, *II* — pre-melting and partial melting, *III* — melting on the depth up to 1 mm [34]

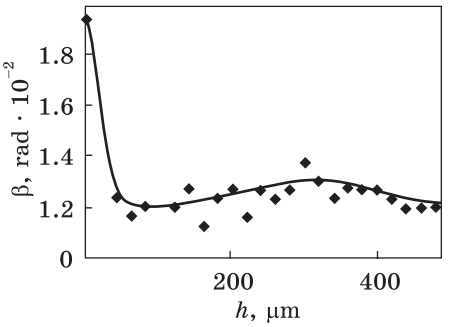

Fig. 11. Dependence of the half-width β of $(211)_{\alpha}$ reflex on the depth of near-surface layer of substrate steel with ESC [17]

of mechanical-pulse treatment. By analogy, we can assume that in our work, the generation of dislocations in the EST process initiated the carbon saturation of the surface layers and the resulting formation of a layer of high-carbon austenite. Tensile residual stresses can also be factors that can initiate diffusion processes [41].

The mechanism of accelerated diffusion in a structurally stressed system can be represented as follows. Local stretched volumes of material can act as acceptors of electrons or individual negatively charged atoms, and compressed volumes can act as donors of positively charged atoms. In this case, the internal stresses will lead to diffusion flows and the resulting mass transfer from compressed to stretched volumes.

Laser heating with an energy density of up to 0.6 J/mm² increased the density of dislocations in the phase components due to the subsequent rapid cooling at a rate of 10^5–10^6 deg/s, which was in the nature of quenching. Because of laser melting, the dislocation density for Fe_{α} and TiC increased to $5.5 \cdot 10^{10}$ cm^{-2} and $6 \cdot 10^{10}$ cm^{-2}, respectively. In the austenitic layer, as in the relaxed phase component of the surface layer, the ρ value increased slightly. W and W_2C practically did not change their dislocation structure under LT.

Thus, in the ESC among the phase components after laser melting, the most significant hardening due to the increased dislocation density

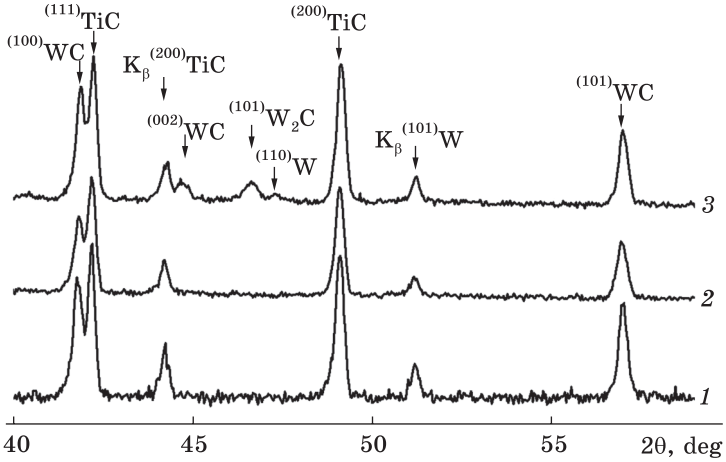

Fig. 12. X-ray pattern of electrode alloy after LT with different energy density: *1* — initial alloy, *2* — 0.25 J/mm², *3* — 0.35 J/mm² [42]

is able to obtain TiC carbide. In the near-surface layer of the steel substrate, the Fe_α component was strength much more than the Fe_γ component.

It should be noted that the calculation of ρ from the value of the physical half-width of x-ray reflexes could be considered correct only if the chemical content of the phase is constant during treatment. Changing the chemical content of the phase can lead to a significant error in ρ determining. For example, the presence of embodiment atoms in a solid solution causes an increase in the physical half-width of the reflex (carbon in martensite). During EST and LT, the components Fe_α and Fe_γ were saturate by carbon due to the ascending diffusion from the steel substrate and the dissociation of the carbides of the doping electrode. The TiC compound also changed its chemical content in the direction of the formation of a complex TiCNO solid solution. Therefore, for these components, the ρ value should be considered as estimated.

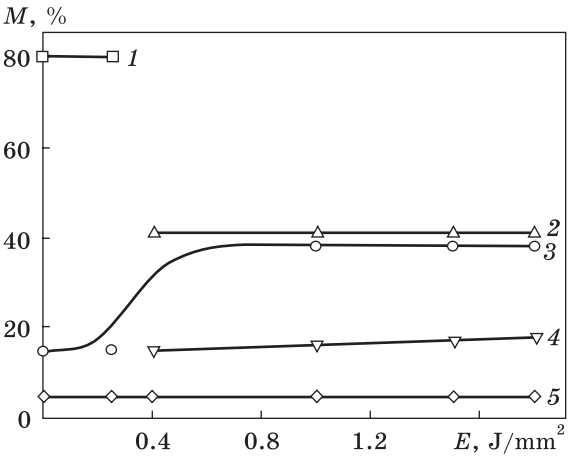

Fig. 13. Phase content of the electrode alloy *vs.* the energy density of laser beam: *1* — WC, *2* — W_2C, *3* — TiC, *4* — W, *5* — Co [17]

LT improves the mechanical properties of ESC. At the same time, due to

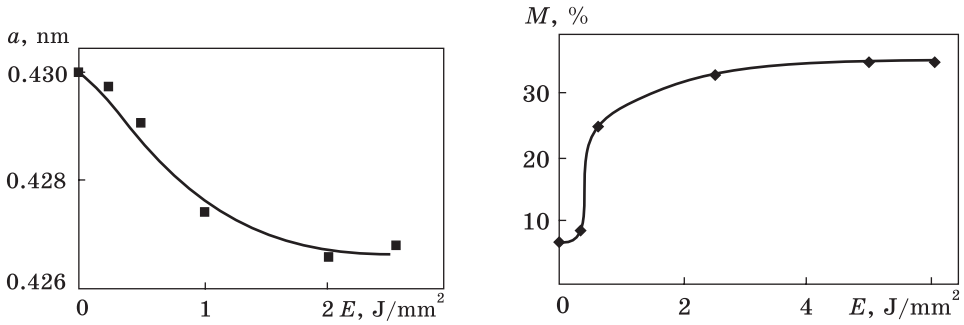

Fig. 14. Change the lattice parameter of the solid solution on the base of TiC in the initial electrode after LT with different energy density of laser beam [43]

Fig. 15. The austenite amount in steel substrate as a function of the energy density of laser beam [43]

the small thickness of the ESC and its discontinuity, laser heating also affects the structural state of the steel substrate. This, in turn, contributes to the formation of the integrated physical and mechanical properties of hardened steel under ESC. In this regard, it is of interest to study the effect of LT on the structural-phase content of the electrode alloy and substrate steel.

Figure 12 shows the changes in the diffraction pattern of the electrode alloy after LT with different energy density of the laser beam. At 0.35 J/mm^2, WC was decomposed into W_2C and pure tungsten [42]. During laser melting, an increase in the TiC content by 20% compared to the initial state was observed (Fig. 13) [17]. The molten surface turned out to be quite fragile. Cracking and destruction of craters took place, the reason for which was a decrease in the plasticizing effect of the addition of cobalt, which dissolved in the austenitic layer (Fig. 14) [43]. This may be due to the formation of the TiCNO compound through the uptake of nitrogen and oxygen from the atmosphere. A characteristic feature of this is the craters of golden colour formed after melting. The last fact testified the intensive nitriding in the mode of laser melting.

For comparison, the structural state of the initial steel substrate (without prior EST) after laser melting investigated. Laser heating caused the formation of residual austenite up to 30% (Fig. 15) [43]. In the initial substrate steel before LT recorded no more than 8% of residual austenite. The increase was due to the dissolution of carbide particles. Some decrease in carbon content observed for the α-phase (Fig. 16, curve *1*) [43]. The physical half-width of the reflex (211) in the α-phase (Fig. 16, curve *2*) increased to almost the same value as in the case of LT steel with ESC (Fig. 10, curve *1*).

LT in the melting mode stabilized austenite in the surface layer with a thickness of 150–300 μm and in alloys where martensitic transformation

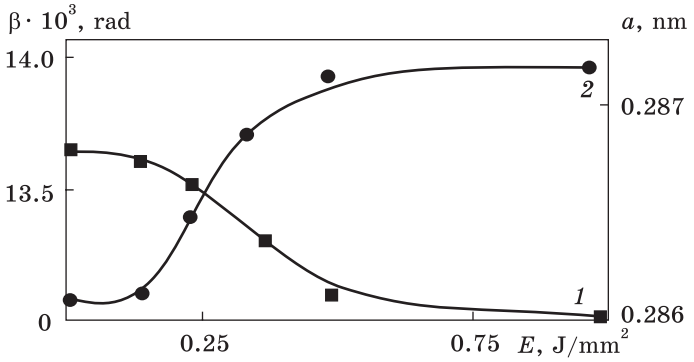

Fig. 16. Lattice parameter (*1*) and physical half-width of $(211)_\alpha$ reflex (*2*) in steel substrate *vs.* the energy density of laser beam [43]

occurred during subsequent cooling to temperatures below room temperature. For example, for alloy Fe–26 wt.% Ni–0.45 wt.% C temperature of martensitic transformation decreased by 20 °C, and the amount of martensitic phase under cooling in liquid nitrogen decreased by 20%.

LT of the steel after EST additionally strengthened the steel substrate because the coating is always discontinuous, and the laser beam reaches the substrate directly in areas that not contain the coating. For these reasons, the yield strength σ_{02} of the reinforced layer of steel 3 was estimated taking into account the experimental values of structural factors.

The value of σ_{02} can additively added as the sum of the components that depend on the degree of dispersion of the structure and the density of dislocations [44]. The first component was determined from the Hall–Petch equation. The grain sizes were choosing from a histogram of dimensions at a certain depth of the layer of laser influence. Calculations showed that the value of σ_{02} varied from 300 to 220 MPa by the depth of the molten layer.

To determine the component of the dislocation density used the expression $\sigma_{02} = MaGb\rho^{-1/2}$, where G is the shear modulus, M is the Taylor factor, a is constant, b is the Burgers vector, ρ is the dislocation density calculated from the physical half-width of the diffraction reflex $(200)_\alpha$. The density of dislocations was in the range $(3.8–8)\cdot 10^{-14}$ m^{-2}. This determined the value of σ_{02} in the range of 260–365 MPa. The total value of σ_{02} of the surface molten layer was 530–600 MPa, which is more than 2.5 times the yield strength of the source material. Thus, the increase in σ_{02} because of laser melting of steel was close to the hardening from phase hardening or to the deformation hardening with a high degree of deformation.

These transformations, which changed the structural state of steel by laser melting, can be considered as components of the process of forming the near-surface layer of the steel substrate because of successive EST and LT.

In further studies, it is advisable to investigate additionally the effect of EST and LT on the structural state of carbon alloys [45–47].

3.4. Regularities of the Residual Stress Formation in the ESC

During the formation of the ESC, the coating thickness is limited by secondary erosion from the cathode and significant tensile residual stresses at the boundary of coating-substrate. Sharply nonequilibrium conditions of the formation of structural-phase state of the ESC and the alloyed layer of steel substrate lead to a significant value of residual stresses σ_r. The main regularities of the distribution of σ_r in coatings under high-energy treatment, including EST, have been sufficiently studied [8, 48]. However, in the works known to us, the σ_r was measured for the main structural component of the coatings and the near-surface layer of steel substrate, which does not allow the total characterization of their complex stress state. In heterophase coatings, it is expedient to measure the σ_r in each of the phase components due to the significant difference in their thermal properties, modulus of elasticity, coefficients of thermal expansion and volume effects during structural transformations. Such selective measurements in different phases can perform only by non-destructive x-ray method. The mechanical Davydenkov's method gives the average values of σ_r for the entire volume of the coating and is not acceptable for measurements in different phase components.

X-ray investigations of the ESC surface showed that the coating material is in a complex structural stress. The formation of tensile stresses of ESC on steels with maximum values on the surface has been reported in the literature [8]. The result was the formation of microcracks in the coating, which propagated in a direction perpendicular to the surface.

In our experiments, it was shown that the stresses in the main phase components differed in both magnitude and sign. For example, tensile stresses of up to 150 MPa were recorded in the TiC-based compound, but in W and W_2C there were already compressive stresses of 70 and 200 MPa, respectively. The content of tungsten in the coating at different EST modes reached 30–40%, so the specific contribution of the stresses developed in tungsten in the overall stress state of the coatings may be significant. This contribution must be taken into account when developing technological modes aimed at relaxing unwanted softening tensile stresses in the ESC, such as surface plastic deformation, which is widely used in the engineering industry to increase the operational reliability of details.

It should be noted that the conditions for determining the residual stresses in the different phase components were significantly different

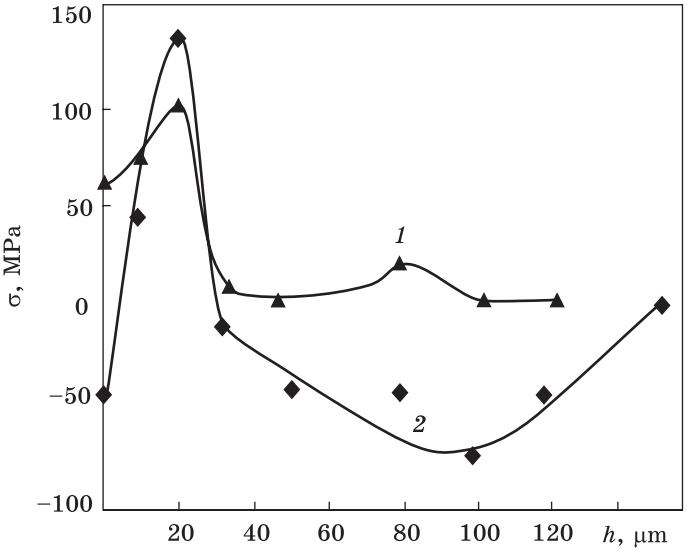

Fig. 17. Stress distribution on depth of the ESC and near-surface layer of the steel substrate: *1* — TiC, *2* — Fe_{α} (coating mode parameters: 1.8 A, 5 min). Chemical etching and mechanical grinding were applied for removing the layer at $h \leq 20$ μm and $h > 20$ μm, respectively [42]

due to the fact that their distribution in the depth of coverage was uneven. Measurement of σ_r in the TiC and W phases was performed by x-ray diffraction of the ESC surface in cobalt radiation. However, under these conditions, it is impossible to measure reliably the σ_r in W_2C. At the inclinations of the sample already at 5–10°, necessary for the implementation of the $\sin^2\psi$ method, the intensity of the reflex $(110)_{W_2C}$ decreased sharply and its angular position due to the partial overlap of the adjacent reflex $(110)_W$ could not be determined with sufficient accuracy. This was due to a decrease in the depth of penetration of cobalt radiation into the coating material under the conditions of the geometry of x-ray at an angle. This fact indicated that the W_2C phase was located in the ESC at some depth inaccessible to cobalt radiation for x-rays at an angle. Therefore, to measure σ_r in W_2C, more rigid x-rays of a molybdenum tube penetrating into tungsten and titanium to the depths of 8 μm and 300 μm, respectively, were used [15]. Measurement of σ_r in the TiC and W phases by x-ray in cobalt and molybdenum radiation showed a difference in the value of σ_r up to 10–15%. This difference was not an experimental error, but was due to the uneven distribution of these phases in the depth of the ESC. The described features of the observation of W_2C and W reflexes indicated that the W phase was located mainly in the near-surface ESC layer, and the W_2C phase distributed at a greater depth of coverage. This is due to the different erosion ability of W_2C and W, which were already released on the surface of the alloying electrode because of WC carbide dissociation.

It was not possible to reliably measure the stress at the depth of the ESC due to its small thickness, but measurements after mechanical pol-

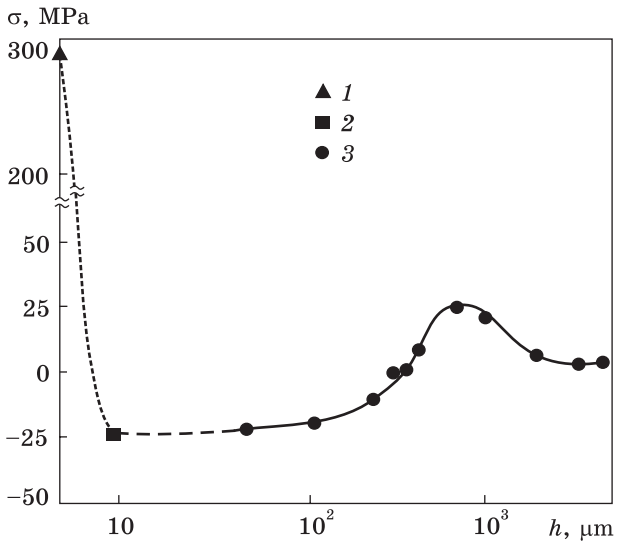

Fig. 18. Distribution of residual stresses over the depth of steel substrate with ESC (treatment mode — 0.8A, 2 min). *1* and *2* — stresses in TiC and Fe_α; measurements were performed on reflexes $(220)_{TiC}$ and $(211)_\alpha$, respectively, during x-ray investigation of surface. *3* — stresses in Fe_α; measurements were performed on the reflex $(211)_\alpha$ during x-ray investigation of the sample edge [42]

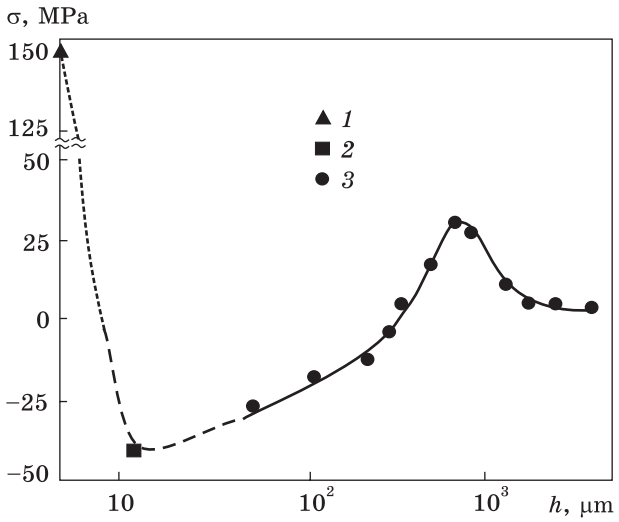

Fig. 19. The same as in the previous figure, but for other coating treatment parameters: 1.8 A, 5 min [42]

ishing and chemical etching showed that the maximum value of both tensile and compressive stresses were on the surface of the coating. Already at a depth of 5–8 μm, the stresses decreased significantly (Fig. 17).

During the x-ray studying of the surface of treated samples, due to the significant discontinuity of the coating on the diffraction pattern the reflexes from the steel substrate were also detected in addition to the main reflections from the coating material. As a result, it is possible to measure the stresses in phase components of the alloy layer without breaking the coating and layer-by-layer etching, which would lead to partial stress relaxation and distortion of the true picture of stress state

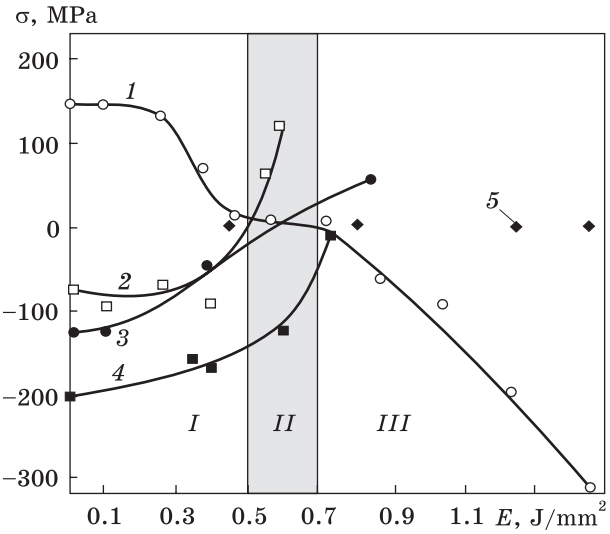

Fig. 20. The value of residual stresses in the phase components of the ESC and steel substrate *vs.* the energy density of the laser beam. Here, *1* — TiC, *2* — W, *3* — Fe_α, *4* — W_2C, *5* — Fe_γ (coating treatment mode — 2.8 A, 5 min); *I* — non-melted zone, *II* — zone of premelting and partial melting, *III* — melted zone; W_2C — (002), W — (110), TiC — (200), Fe_α — (200), Fe_γ — (200) [34]

of the alloy layer. It turned out that in the α-phase of the steel substrate under all treatment modes only compressive stresses developed. A more intensive coating mode (increasing the magnitude of the electric current and the duration of treatment) led to an increase in compressive stresses in the α-phase. The x-ray investigations of the end face of the sample revealed that the compressive stresses in the α-phase gradually changed to tensile on the depths of the steel substrate to 70–80 μm (Figs. 18 and 19).

Laser heating can significantly change the structural state and nature of the distribution of residual stresses not only ESC but also steel substrate, in particular, lead to the formation of austenite in armco iron and in carbon steels the amount of residual austenite increase [49–53]. It was previously shown that LT partially eliminated the imperfections of the ESC. The combined effect of EST and subsequent laser heating allow increasing in several times the depth of the strengthened layer, reduce the distribution gradient of alloying elements, physical and mechanical properties, reduce residual stresses, and detect and even eliminate the imperfections (defects) naturally present in the coatings [54–59] as well as in the alloys in whole [60–66].

Figure 20 shows the change in the stress state of the ESC and the near-surface layer of the substrate after LT [42]. A noticeable decrease in stresses began when heated by a laser beam with an energy density of 0.3 J/mm^2. Both tensile stresses in TiC and compressive stresses in W, W_2C, and Fe_α were relaxed. In the region of pre-melting (energy density varies from 0.45 to 0.7 J/mm^2) stresses in TiC, W and Fe_α relaxed almost completely. The stresses in the W, which did not reach melting, changed sign in this region and became tensile with a value close to the value of the stresses in the TiC phase of the initial ESC (before laser

heating). They were purely thermal stresses, not associated with structural changes in the coating. For W_2C, stress relaxation was observed at energy densities of 0.7 J/mm^2.

Thus, in the pre-melting mode in the ESC and the doped layer, the residual stresses were relaxed in almost all components, except W_2C, while maintaining the phase content formed during EST. All that remained were the compressive stresses in the W_2C, which had a strengthening character. More intense heating caused melting of the ESC and the partially doped layer of the substrate with convective mixing of their components and the formation of a new-doped layer with a different structural-phase state.

In the layer formed in this way, pure tungsten was no longer fixed. According to Ref. [21], tungsten is soluble in Fe_γ up to 6%. Therefore, we can assume that it was partially soluble in austenite, and formed a highly dispersed carbide phase. The transition of tungsten to other phases contributed to the relaxation of tensile stresses that occurred in tungsten when heated, which provided melting of the coating. Tensile stresses were formed in the Fe_α phase and compressive stresses in the TiC phase. In this case, in the entire range of the laser beam influence, as already mentioned, the austenitic phase did not contain stresses, remaining a relaxed layer in the stressed heterophase system.

When LT in the melting mode, the stress state of the system was determined only by the energy density of laser beam, and the effect of the previous EST affected mainly in the formation of the initial phase content of the coating. Thus, ESC melting led to the formation of a qualitatively new structural-stress state with a new set of physical and mechanical properties.

3.5. The Reverse α–γ Transformation in the Near-Surface Layers of the Steel Substrate

Under all EST regimes, a thin layer of austenite was formed in the substrate steel. Microstructural studies showed that the thickness of austenitic layer did not exceed 40–60 μm. From the ratio of the integrated intensity of the reflexes $(200)_\gamma$ and $(110)_\alpha$, it was found that depending on the electrical mode of coating, the austenite content in the surface layer of steel ranged from 20 to 90%. During the photoregistration of the diffraction pattern on the x-ray film, differences in the intensity of austenitic reflexes in the azimuthal direction were observed, which indicated a certain distribution of austenitic grains by size and crystallographic orientation (grain size was 10–20 μm). In addition, this intensity ratio differed from the theoretical one, which was due to some texture that arose during the rapid crystallization of austenite from the melt. The parameter of the austenite lattice a_γ was fixed in the range of

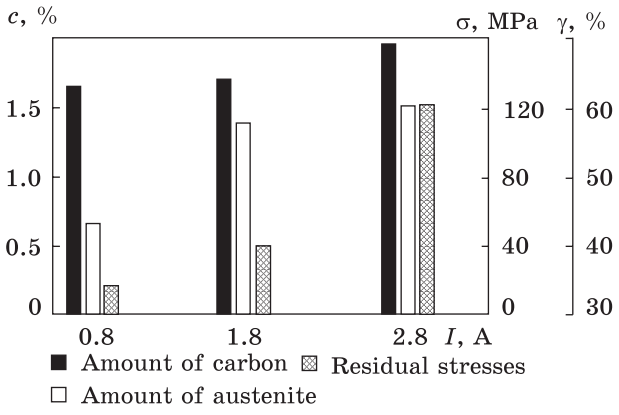

Fig. 21. The compressive stresses' magnitude σ in α-phase, the austenite amount γ and carbon content *c* in it *vs.* the current value current *I* (for 2 min of the ESC process) [17]

0.3580–0.3645 nm. The value of a_γ depended not only on the content of carbon, but also on the content of cobalt and tungsten dissolved in Fe_γ at high temperatures. The content of carbon in austenite, determined by the a_γ parameter, was equal to 1.2–2 wt.%. Increasing the intensity of EST led to an increase in the amount of austenitic phase and a simultaneous increase in the content of carbon in it (Fig. 21) [42].

Cementite in the alloyed steel layer was not observed by x-ray due to its high dispersion and small amount. However, it could be observed after electrolytic isolation, as well as in an electron microscope for carbon content in the surface layer of more than 1% [55].

Significant enrichment of the surface layer by carbon was recorded by x-ray spectral method. Carbon came into the surface layer from the discharge channel as a product of dissociation of TiC and WC, as well as from the lower layers of the steel substrate by the ascending diffusion mechanism. The carbon-enriched layer lay at some depth from the surface.

When melting the surface layer of the substrate, it is also necessary to consider the possibility of dissolving air nitrogen in γ-iron. As reported in Ref. [56], nitrogen can be introduced from the plasma jet into the metal melt in amount significantly exceeding the equilibrium for normal melting conditions while maintaining the partial pressure of nitrogen in the gas phase. In the process of LT, there was a gas breakdown and a plasma torch was formed near the melted surface. As a result, the metal melted by the laser beam was able to absorb intensively the nitrogen from the atmosphere [57, 58]. Since the processes of plasma formation by EST are to some extent similar to the processes by laser, plasma and electric arc treatment, it can be assumed that, because of EST, the surface melt of the steel substrate can be saturated by nitrogen from the atmosphere. The emergence of a high-pressure zone under pulsed electric discharges, as well as under pulsed laser heating,

contributed to the dissolution of nitrogen in a metal liquid bath [58, 59]. Therefore, the increased austenite lattice parameter a_γ after EST was determined by dissolved atoms of both C and N. The dependence of a_γ is close to the content of carbon, c_C, and nitrogen, c_N, in the γ-solid solution [67]: $a_\gamma = 0.3556 + 0.00095c_C$ and $a_\gamma = 0.3566 + 0.0008c_N$.

From the last two expressions, we can assume that the value of 1.2–2 wt.% embodied atoms in the austenite lattice corresponds to the total carbon and nitrogen content in the γ-solid solution (the effect of Co and W on the a_γ parameter not taken into account).

An interesting feature of the structural state of the doped layer was the almost complete relaxation of stresses in the austenitic phase. The austenitic layer under the studied treatment modes, regardless of its thickness and carbon content in it, had virtually no residual stresses. It can be assumed that the relaxation of stresses in the austenitic phase was associated with a decrease in the specific volume of the phase during the reverse α–γ transformation. The detected phenomenon can be technologically useful because such a layer was formed directly under the ESC and relaxed stress at the coating–substrate boundary. These stresses reduced the adhesion of the coating material and steel substrate, and thereby limiting the thickness of the coated layer.

During the intensive treatment, more significant stresses are developed at the boundary with the substrate. At the same time, the relaxation capacity of the austenitic layer increased. This was determined by the increase in the volume effect of α–γ transformation with increasing carbon content. It was found that the dependence of the volume effect of α–γ transformation on the amount of carbon in steel could be expressed as [68] $(\Delta V/\Delta V)_{\alpha-\gamma} = 2.5 + 1.08c_C$ (c_C is in wt.%). The above expression can also indirectly characterize the degree of stress relaxation by the austenitic layer with increasing of carbon content in it. The plastic austenitic layer, obviously, is able to play the role of a buffer between the substrate and the fragile components of the coating under microshock mechanical loads during operation of parts with wear-resistant coatings.

In order to realize the martensitic transformation in the austenitic phase, which could lead to additional strengthening of the subsurface layer of substrate by increasing the amount of α-phase, the sample with ESC was cooled in liquid nitrogen. It turned out that the phase content of both the ESC and the surface layer of the substrate did not change. However, the intensity of γ-phase reflexes decreased slightly, and they became more blurred (Fig. 19) [42]. This indicated a weak γ–α transformation in the austenitic layer. To observe a clearer diffraction pattern of the austenitic layer, the ESC samples were ground to remove the coating material. It is known that the martensitic transformation in steel with 1.5–2 wt.% C begins at temperatures of 90±20 °C and ends

at a temperature of approximately −100° C. In our experiments, the γ–α transformation in austenitic grains was not realized when the samples were cooled to –196 °C. This indicated that Co and W also dissolved in austenite, in addition to carbon, which lowered the martensite point below the temperature of liquid nitrogen.

3.6. Influence of Erosion Mechanism on the ESC Formation

Microstructural studies have shown the unevenness of the ESC thickness and its significant discontinuity [34]. Some areas of the substrate did not contain the coating material. The discontinuity of the coating reached 20–25%. This was confirmed by x-ray diffraction, when reflexes were recorded from the steel substrate, which would be completely absorbed in the coating in the case of its continuity. In the microstructural image under the coating, an austenitic layer of 40–60 μm thick was pronounced. The boundaries of the coating-austenitic layer-substrate formed quite clear and the noticeable transition layers were not detected.

In the microstructural images it were clearly separated the areas of the applied coating (white layer), the average thickness of which varied from 20 to 80 μm, and in some places it was possible to obtain the individual sections of ESC with a thickness of 100–120 μm. The microstructure of the applied white layer was not studied in detail due to its insufficient chemical activity. Previously, this was accurately done in Ref. [69].

It observed the unevenness of the coating, as well as the porosity of the applied layer in places with greater thickness. At smaller thicknesses, a more uniform distribution of the coating components was observed. The white layer is characterized by high microhardness compared to the steel matrix. The thickness of the applied layer did not affect on the microhardness of the initial steel substrate, but the microhardness of the austenitic layer was slightly higher compared to the lower region of the initial matrix. Figure 22 shows the change of microhardness of the ESC and steel substrate on depth.

X-ray spectral analysis on the 'Jeol Superproble' equipment showed the different distribution of elements in the substrate material. The image in the secondary electrons showed that the formation of the coating took place by successively increasing it due to the mass transfer of individual solid particles or droplets. Noticeable sharp seams between the layers of the coating. The coating has a pronounced surface relief. The austenitic layer was thin and not always solid. In some cases, it has been observed that it has thinned in areas where there was practically no coating material containing carbon. It follows from the fact that enrichment of the near-surface layer of the substrate by carbon and the formation of the γ-phase occurred due to its diffusion from the coating,

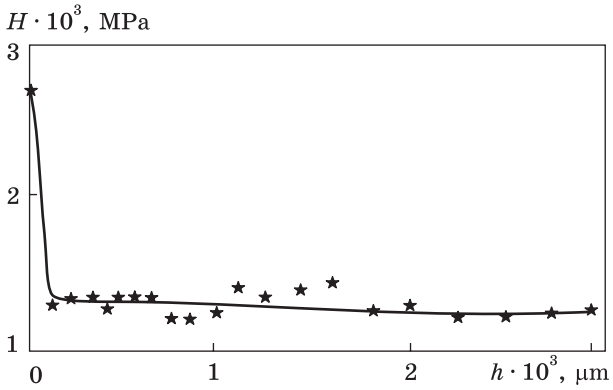

Fig. 22. Microhardness of the ESC *vs.* the steel substrate depth [28]

and not only due to the ascending diffusion from the layers of the substrate below.

It was observed the different nature of the redistribution of elements of the coating material and the substrate - tungsten and cobalt penetrated into the near-surface layer of the substrate, and iron - in the coating material. The protrusions of the relief and the near-surface layer of the coating were depleted of iron. Cobalt is most evenly distributed in the coating. Tungsten accumulated unevenly on the substrate. In the near-surface layer of the coating, its amount was greater than at some depth. The mass transfer of tungsten was associated with its erosive ability. Because of this, tungsten was released on the electrode as a product of WC dissociation. Titanium was distributed unevenly; one could see the individual round formations. These were obviously traces of liquid droplets against a more even distribution over the volume of the coating. The upper coating layer up to 5–7 μm thick was depleted titanium. This indicated the non-monotonic nature of mass transfer from the electrode alloy. The coating material contained the round inclusions. They can be considered as solid-state particles melted in the interelectrode gap. Such particles were formed due to the fragility of the TiC compound caused by a significant proportion of covalent bonds in its structure.

Not only mass transfer causes significant enrichment by the carbon of the upper layer of coating with a thickness of 16–20 μm from the electrode, but also ascending diffusion from the substrate. The form of image of the coating in the radiation of TiK_α, CoK_α and WL_α differed noticeably. This suggests that carbon, which is contained in the coating, is not all in the carbide of TiC or W_2C. At some depth of the coating, it is included in the γ-solid solution of the substrate.

Elements of phase components that participated in structural transformations are distributed unevenly by crossing the coating. The nonmonotony of the mass transfer in the EST process is associated with phase transformations and components of the erosion mechanism.

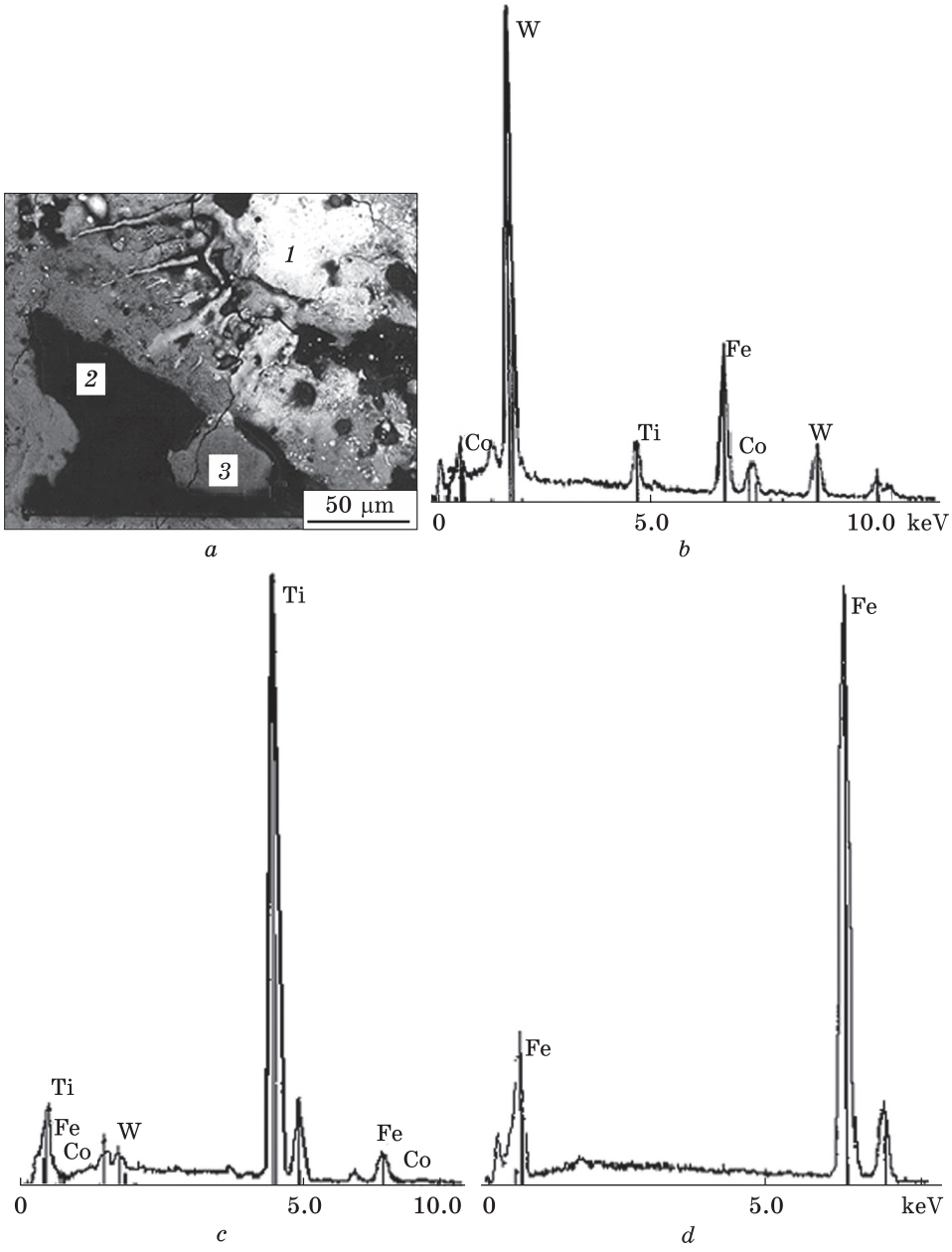

Fig. 23. The ESC microstructure at an early formation stage (*a*), where *1*, *2*, and *3* denote regions of the spectra (*b*–*d*) [70]

Additional information about the microstructure of coatings was obtained by scanning electron microscope 'Philips'. The microstructure of the coating was analysed at an early stage of its formation. This al-

lowed tracing the formation of separate substructural elements responsible for which could be the components of the erosion mechanism. The formation of the coating occurred by precipitation on a substrate as liquid drops and solid-state particles (Fig. 23, *a*) [17]. Drops were precipitated on a substrate with noticeable spraying. At this, the branches of the main drops in the form of the thin narrowed 'moustaches' were formed. Some of them were interrupted because of a significant impulse mechanical blow of the drop on the surface. The cooling rate of the 'moustaches' material was significantly higher due to their smaller mass than the cooling rate of the material of the main drop. Because of it, in the 'moustaches' the high internal stresses formed and relaxed by cracks. The cracks also occurred in the coating material formed during the precipitation of the main drop, as well as in the areas of the substrate without coating. Obviously, the conditions of condensation of the 'moustaches' materials are approaching to the conditions of spinning, which used in obtaining of highly dispersed and amorphous ribbons. Therefore, it can wait for partial amorphization of the 'moustaches' material when material contents the amorphyzing elements.

The study of local regions showed the differences in the chemical content in various components of the coating. In the dark formation, formed during realization of the solid-state mass transfer mechanism, the spectrum showed the highest content of titanium and only traces of cobalt. In the spectrum of the grey microstructure zone, iron lines recorded (Fig. 23, *c*, *d*). In this area during EST the coating not formed.

The results of this study of the coating confirmed the idea of the erosion mechanism [8]. The fraction of the coating in the incorrect embedded form with blurred edges by the partial melting (Fig. 23, *a*) indicated of the mass transfer mechanism of TiC phase due to its fragile destruction caused by a significant proportion of covalent bond. For phases that contain tungsten the erosion in the liquid phase characterized (Fig. 23, *b*).

As shown in Fig. 24, the large inclusions formed by the implementation of the mechanism of liquid-metal erosion [28]. A characteristic feature of the formations of a drop fraction containing tungsten is a clearly expressed system of grain boundaries, along which the point excretions is visible. There were also the unclosed and discontinuous boundaries with excretions. Identification of these excretions failed.

LT of the coating in the mode of its melting aligned the relief and formed a new one of specific character. The surface of the coated samples was melted by consistent laser pulses with overlap of laser spots by 10–15% (Fig. 23, *a*) [70]. In the centre of spots, there were cracks that spread radially on the melting zone. X-ray investigations showed the presence of significant residual stresses with a maximum in the centre of the spot.

After laser melting, the holes observed in the centre of melted zone. In this case, the surface of the holes had a golden colour characteristic of the TiN compound. Increasing the density of laser beam energy caused the formation of a crater due to the emission of evaporated material. In the zone of laser spot, the concentric circles observed to be considered as crystallization waves of the melt, which hardened at high cooling rate (Fig. 23, *b*). On the periphery of the laser spot, dark formations are visible, obviously, in-melted and pressed out during the crystallization of zone. The tenfold increase in the region of crystallization waves showed its cellular structure with separate formations of 1–3 μm (Fig. 23, *c*).

Spectral analysis of large dark formations on the periphery of laser spot (Fig. 24, *a*) showed the presence in its content of a significant amount of tungsten and iron (Fig. 24, *b*) [70]. This indicated the formation of steel carbide Fe_3W_3C. Indeed, on the ESC diffraction pattern, a reflex with an angle of reflection $2\Theta = 70.85°$ was fixed, which can be attributed to the $(551)_{Fe_3W_3C}$ reflex. Other intensive reflexes of this carbide coincided with reflexes of W_2C carbide and austenite, e.g., reflex $(422)_{Fe_3W_3C}$ was superimposed on $(101)_{W_2C}$, while $(553)_{Fe_3W_3C}$ practically coincided with (220). In the ESC, the content of W, Ti, Co, close to their contents in the initial electrode, was detected by the x-ray spectral method.

An attempt to monitor the distribution of nitrogen in the ESC by x-ray spectral method was unsuccessful. This was due to the fact that the spectral line of nitrogen $K_{\alpha 1}$, corresponding to a wavelength of 3.16 nm, has practically coincided with more than order intensive line of cobalt $L_{\alpha 1}$, which corresponded to a wavelength of 3.18 nm. It coincided with the titanium line $L_{\alpha 1}$ (wave length 3.134 nm), but the last has an intensity less in order of magnitude than the intensity of the corresponding cobalt line and it could be not taken into account [71].

The nitrogen content in the ESC was determined by a photocolometric method using a Nessler reagent [72]. Due to the difficulties associated with the removal of the ESC material without a substrate material, nitrogen was detected in amount that did not exceed the tenths of wt.%. The low content of nitrogen was explained by presence in the removed material of a large amount of substrate material. After LT of the ESC, these difficulties could not be avoided. Further, as analysed on nitrogen content, the basic component of the initial electrode alloy or ESC (TiC carbide) is capable to assimilate the nitrogen from atmospheric air. For this purpose, TiC powder treated by a laser beam in melting mode. In this mode of treatment, the powder was sprayed because of mechanical impulse that arose when absorbing of a laser beam. Therefore, treatment of powder carried out under a quartz plate that pressed powder and was transparent for a laser beam with a wavelength of 1.06 μm. The sintered powder was dissolved for 30–40 h in a reagent of 5 ml

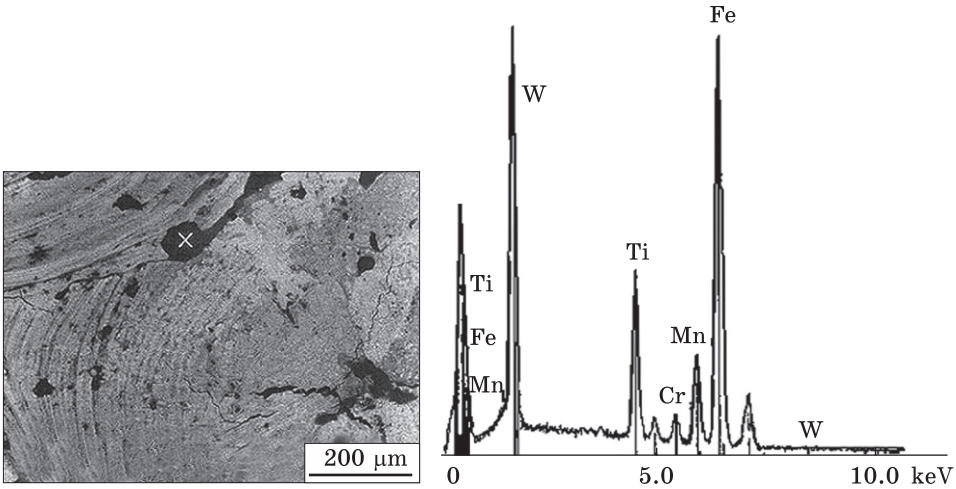

Fig. 24. Carbide particle at the laser spot overlap boundary (*a*) and corresponding spectrum (*b*) [70]

{H_2SO_4 (1–4 water) + 25 ml of HF (1–5 water)} + 1 ml of hydrogen peroxide. The dissolution products collected through a water shutter in weak acid and overflowed by alkali. The formed ammonia was distilled off and by the optical density of the solution it was determined the content of nitrogen. It turned out to be 0.62 wt.%. It should assumed that the content of nitrogen is significantly underestimated, because it absorbed only by melted surface layer of the TiC carbide powder, and the calculation was relatively to the whole volume. Indeed, x-ray of the ESC, as well as its surface after laser melting showed that a decrease in the TiC lattice parameter corresponded to the formation of 20–40% TiN compound in a solid solution of TiCN.

LT of the TiN compound in atmospheric air is possible in addition to nitrogen, as well as oxygen, which is capable to form a solid solution with titanium. In this case, it can assume that a solid solution of TiCNO formed by laser melting. The ability to dissolve the gases in the titanium fell in the TiC–TiN–TiO sequence. The presence of an insoluble residue indicated the presence of TiO in samples of TiC carbide samples after LT.

For comparison, it should be noted that LT of the carbonic Fe alloys causes some other qualitative effects of the formation of a structural-phase state [73–75].

4. Summary and Conclusions

At the initial stage of EST in the near-surface layers of the electrode alloy proceeded the dissociation of WC carbide on components of W_2C and W and their further erosion with the following formation of the

ESC on substrate steel. In the ESC material, traces of WC are not detected due to its practically complete dissociation on the electrode. In the inter-electrode environment based on the TiC carbide, the TiCN carbide was synthesized due to the absorption of nitrogen from atmospheric air. A significant amount of plasticizing component (cobalt) dissolved in other components of the coating and substrate.

As a result of these processes, the phase content of the coating differed significantly from the content of the electrode alloy. It turned out to be quite sensitive to the EST and the next LT. Thus, with an increase in electric current of discharge or density of the energy of laser beam, the amount of W_2C carbide in the coating increased, and the proportion of TiN in TiCN carbonitride increased to 70–80%. The formation of these components has strengthened the coating.

The study of microstructures in the early stages of the ESC formation, by means of a scanning microscope with a microprobe, allowed establishing as follows. The TiC emerged in a solid phase with a partial surface melting due to a significant proportion of covalent bond in this compound, which is known to be responsible for fragile destruction and subsequent mass transfer in a solid phase. Fractions of the coating in the form of particles of irregularly grabbed form gave a spectral pattern with an intense Ti-line. The mass transfer of the tungsten components W_2C and W was due to a liquid-drop mechanism. This indicated the formation of the component of coating in the form of a sprayed crystallized drop, the spectrogram of which contained an intensive W-line.

Deposition on a substrate as a liquid drop, as well as solid-state particles confirmed existing ideas about the mechanism of erosion and formation of the ESC associated with the nature of the interatomic bond in the material of doping electrode.

For the first time, the possibility of secondary carbidization of tungsten in the ESC formed by the dissociation of WC carbide and worsened the mechanical properties of the coating. With the participation of ascending diffusion of carbon from a substrate, W_2C carbide formed, starting from a certain depth of coating. Secondary carbidization occurred in the near-surface layer of coating by the next LT. By the depth of the ESC, the amount of W_2C carbide increased by 25%, and for the next LT — by 30%. Additional W_2C formation significantly increased the microhardness of the ESC.

The structural-phase state of the steel substrate after EST has also changed significantly. Due to the mutual diffusion of the coating elements and substrate and the ascending diffusion of carbon in the transition region, a highly-alloy austenitic layer and a fast-cut steel Fe_3W_3C carbide was formed.

In the EST process, a complex structural-stress state of the heterophase coating and a substrate formed. Residual stresses in various

phase components were different not only in magnitude, but also by a sign. The tensile stresses are formed in the TiCN, whereas the compressive ones are formed in the constituents W_2C, W, and Fe_α. In the austenite layer, the residual stresses were practically absent due to the implementation of reverse martensitic α–γ–transformation, which proceeded with a decrease in the specific volume. During intensive EST, the relaxation capacity of the austenitic layer grew. This was determined by an increase in the volumetric effect in the α–γ transformation with increasing C content in the γ-phase. Relaxation of stresses contributed to reducing them on the interphase border and growth of ESC thickness.

The possibility of selective relaxation of residual stresses in various phase components of the ESC with help of the next LT have found. Laser heating of the coating is capable to improve its operational properties by increasing the proportion of TiN nitride in TiCN carbonitride, formation of high-strength W_2C carbide and relaxation of depleting tensile stresses with partial preservation of strengthening compression stresses. After laser melting, a qualitatively new structural-phase state of the coating formed.

Formation of nitrides and carbonitrides instead of carbide of titanium in the ESC may be useful since as compared to carbides they have a larger microhardness, low friction coefficient on the iron-based alloys and high wear resistance.

REFERENCES

1. X. Wei , Z. Chen, J. Zhong, and Y. Xiang, Feasibility of preparing Mo_2FeB_2-based cermet coating by electrospark deposition on high speed steel, *Surf. Coat. Technol.*, **296**: 58 (2016);
https://doi.org/10.1016/j.surfcoat.2016.03.090
2. A.A. Burkov, S.A. Pyachin, M.A. Ermakov, and A.V. Syuy, In situ synthesis and characterization of Fe-based metallic glass coatings by electrospark deposition technique, *Journal of Materials Engineering and Performance*, **26**, No. 2: 901 (2017);
https://doi.org/10.1007/s11665-016-2493-6
3. S.H. Baghjari, F.M. Ghaini, H.R. Shahverdi, C.M. Barella, and D. Ripamonti, Laser welding of niobium to 410 steel with a nickel interlayer produced by electro spark deposition, *Materials and Design*, **107**: 108 (2016);
https://doi.org/10.1016/j.matdes.2016.06.022
4. R. Yamanoglu, N. Gulsoy, E.A. Olevsky, and H.O. Gulsoy, Production of porous Ti5Al2.5Fe alloy via pressureless spark plasma sintering, *J. Alloys Compd.*, **680**: 654 (2016);
https://doi.org/10.1016/j.jallcom.2016.04.176
5. K. Soma Raju, N.H. Faisal, D.S. Rao, S.V. Joshi, and G. Sundararajan, Electrospark coatings for enhanced performance of twist drills, *Surf. Coat. Technol.*, **202**: 1636 (2008);
https://doi.org/10.1016/j.surfcoat.2007.07.084
6. M. Scendo, N. Radek, and J. Trela, The influence of electrospark and laser treatment upon corrosive resistance of carbon steel, *Adv. Mater. Res.*, **874**: 107 (2014);
https://doi.org/10.4028/www.scientific.net/AMR.874.107

7. D.W. Heard, J. Boselli, R. Rioja, E.A. Marquis, R. Gauvin, and M. Brochu, Interfacial morphology development and solute trapping behavior during rapid solidification of an Al–Li–Cu alloy, *Acta. Mater.*, **61**: 1571 (2013); https://doi.org/10.1016/j.actamat.2012.11.034
8. V.Y. Bondar, V.E. Danilchenko, A.V. Filatov, V.F. Mazanko, and V.E. Iakovlev, Effect of cyclic martensitic γ–ε–γ transformations on diffusion characteristics of carbon in an iron–manganese alloy, *Prog. Phys. Met.*, **19**, No. 1: 70 (2018); https://doi.org/10.15407/ufm.19.01.070
9. V.Yu. Danilchenko, A.V. Filatov, V.F. Mazanko, and V.E. Iakovlev, Effect of cyclic martensitic γ–ε transformations on diffusion characteristics of cobalt in an iron–manganese alloy, *Prog. Phys. Met.*, **20**, No. 3: 426 (2019); https://doi.org/10.15407/ufm.20.03.426
10. P.A. Molian, Structure and hardness of laser-processed Fe–0.2% C–5% Cr and Fe–0.2% C–10% Cr alloys, *J. Mater. Sci.*, **20**, No. 8: 2903 (1985); https://doi.org/10.1007/BF00553054
11. J. Tang, Mechanical and tribological properties of the TiC–TiB2 composite coating deposited on 40Cr-steel by electro spark deposition, *Appl. Surf. Sci.*, **365**: 202 (2016); https://doi.org/10.1016/j.apsusc.2015.12.198
12. M.F. Hasanabadi, F.M. Ghaini, M. Ebrahimnia, and H.R. Shahverdi, Production of amorphous and nanocrystalline iron based coatings by electro-spark deposition process, *Surf. Coat. Technol.*, **270**: 95 (2015); https://doi.org/10.1016/j.surfcoat.2015.03.016
13. V. Bondar, V. Danilchenko, and Ie. Dzevin, Gradient distribution of martensite phase in melt-spun ribbons of a Fe–Ni–Ti–Al Alloy, *Nanoscale Res. Lett.*, **11**: 96 (2016); https://doi.org/10.1186/s11671-016-1313-0
14. A.A. Rusakov, *Rentgenografija Metallov* [X-ray Investigation of Metals] (Moscow: Atomizdat: 1977) (in Russian).
15. L.I. Mirkin, *Spravochnik po Rentgenostrukturnomu Analizu* [Handbook of X-ray Structural Analysis] (Moscow: Gosizdat Phys. Math. Lit.: 1961) (in Russian).
16. A.Yu. Babkevich, V.I. Bondar, and V.E. Danilchenko, *Z. Metallkd.*, **88**: 489 (1997).
17. V.E. Danilchenko, V.I. Bondar, and A.M. Semyrga, *Proc. Int. Conf. 'Oborudovanie i Tehnologiya Termicheskoy Obrabotki Metallov i Splavov'* [Equipment and Technology of Heat Treatment of Metals and Alloys] (Kharkov: 2005), Pt. 2, p. 263 (in Russian).
18. V.Yu. Danil'chenko and O.M. Semirga, *Metallofiz. Noveishie Tekhnol.*, **28**, Spec. Iss.: 361 (2006).
19. A.D. Verhoturov, F.F. Egorov, and M.D. Smolin, *Powder Metallurgy*, No. 9: 28 (1982).
20. G.V. Samsonov and I. M. Vinnickij, *Tugoplavkie Soedineniya* [Refractory compounds] (Moscow: Metallurgiya: 1976) (in Russian).
21. A.E. Vol, *Stroenie i Svoistva Dvoinykh Metallicheskikh Sistem* [Structure and Properties of Double Metal Systems] (Moscow: Gosizdat Phys. Math. Lit: 1959), Vol. **1** (in Russian).
22. O.M. Semyrga, *Zakonomirnosti Formuvannia Structurno-Fazovogo Stanu Pokrytiv ta Prypoverkhnevykh Shariv Splaviv na Osnovi Zaliza i Tytana pry Kombinovaniy Impulsniy Obrobtsi* [Regularities of Formation of Structural-Phase State of Coatings and Near-Surface Layers of Iron and Titanium-Based Alloys in Combined Pulse Treatment] (Thesis of Disser. for Cand. Phys.-Math. Sci.) (Kyiv: G.V. Kurdyumov Institute for Metal Physics of the N.A.S. of Ukraine: 2004) (in Ukrainian).

23. A.S. Bay, D.I. Leiper, and E.N. Slesariova, *Okislenie Titana i Ego Splavov* [Oxidation of Titanium and Its Alloys] (Moscow: Metallurgizdat: 1970) (in Russian).
24. J.F. Ready, Effects due to absorption of laser radiation, *J. Appl. Phys*, **36**, No. 2: 462 (1965); https://doi.org/10.1063/1.1714012
25. P.A. Leontiev, M.G. Han, and N.T. Chekanova, *Lazernaya Poverkhnostnaya Obrabotka Metallov i Splavov* [Laser Surface Treatment of Metals and Alloys] (Moscow: Metallurgiya: 1986) (in Russian).
26. I.V. Kudriavcev, *Materialy v Mashinostroenii. Spravochnik* [Materials in Mashinbuilding. Handbook] T.5 (Moscow: Mashinostroenie: 1969) (in Russian).
27. V.Yu. Danil'chenko and O.M. Semyrga, The phase composition of a hardmetal coating deposited by spark discharge on a carbon steel substrate, *J. Superhard Mater.*, **30**: 188 (2008); https://doi.org/10.3103/S1063457608030064
28. V.E. Danilchenko, V.I. Bondar, and A.M. Semyrga, *Proc. Int. Conf. 'Oborudovanie i Tehnologiya Termicheskoy Obrabotki Metallov i Splavov'* [Equipment and Technology of Heat Treatment of Metals and Alloys], (Kharkov: 2005), Pt. 3, p. 123 (in Russian).
29. V.N. Eremenko, *Mnogocomponentnye Splavy Titana* [Multicomponent Titanium Alloys] (Kiev: Izdatelstvo AN USSR: 1962) (in Russian).
30. I.I. Safronov, *Issledovanie Vozmoznosti Primeneniya Karbidnykh i Boridnykh Soedineniy Titana, Niobiya, Zirkoniya i Khroma v Kachestve Electrodov dlia Electroiskrovogo Legirovaniya* [Study of the Possibility of Using Carbide and Boride Compounds of Titanium, Niobium, Zirconium and Chromium as Electrodes for Electrospark Alloying] (Thesis of Disser. for Dr. Phys.-Math. Sci.) (Kiev: Institute for Problems of Materials Science, AN USSR: 1967) (in Russian).
31. V.M. Schastlivtsev, D.A. Mirzaev, and I.P. Yakovleva, *Structura Termicheski Obrabotannoy Stali* [Heat Treated Steel Structure] (Moscow: Metallurgiya: 1994) (in Russian).
32. A.I. Gordienko and A.A. Shipko, *Strukturnye i Fazovye Prevrascheniya v Titanovykh Splavah pri Bystrom Nagreve* [Structure and Phase Transformations in Titanium Alloys at Fast Heating] (Minsk: 1983) (in Russian).
33. A.E. Gitlevich, G.I. Dimitrova, and T.V. Pushnina, *Electr. Proc. Mat.*, No. 2: 12 (1991).
34. V.E. Danilchenko, V.I. Bondar, Yu.V. Gubin, A.V. Paustovsky, and A.M. Semyrga, *Physicochemical Mechanics of Materials*, No. 5: 115 (2005).
35. M.L. Bernshtejn and A.G. Rahshtadt, *Metallovedenie i Termicheskaya Obrabotka Stali: Spravochnik* [Metallurgy and Heat Treatment of Steel: Handbook], Vol. **1** (Moscow: Metallurgiya: 1983) (in Russian).
36. M.P. Shaskolskaja, *Kristallografiya* [Crystallography] (Moscow: Vysshaya Shkola: 1976) (in Russian).
37. V.A. Andryuschenko, Ye.M. Dzevin, V.F. Mazanko, and V.L. Svechnikov, *Metallofiz. Noveishie Tekhnol.*, **21**, No. 9: 71 (1999).
38. D.S. Gertsriken, V.F. Mazanko, and V.M. Falchenko, *Impulsnaya Obrabotka i Massoperenos v Metallakh pri Nizkikh Temperaturah* [Pulse Processing and Mass Transfer in Metals at Low Temperatures] (Kiev: Naukova Dumka: 1991) (in Russian).
39. V.I. Kiriliv, *Physicochemical Mechanics of Materials*, No. 6: 88 (1999).
40. S.Z. Bokshtein, *Diffuziya i Struktura Metallov* [Diffusion and Structure of Materials] (Moscow: Metallurgiya: 1973) (in Russian).

41. J. Fridel, *Dislokatsii* [Dislocations] (Moscow: 1967) (in Russian).
42. V.I. Bondar, V.Yu. Danyl'chenko, G.I. Prokopenko, and A.M. Semirga, *Metallofiz. Noveishie Tekhnol.*, **25**, No. 4: 485 (2003) (in Russian).
43. V.E. Danilchenko and V.I. Bondar, *Proc. Int. Conf. 'Oborudovanie i Tehnologiya Termicheskoy Obrabotki Metallov i Splavov'* [Equipment and Technology of Heat Treatment of Metals and Alloys], (Kharkov: 2005), Pt. 2, p. 205.
44. V.E. Danilchenko and B.B. Polchuk, *Materials Science Forum*, **378**: 440 (2001) (in Russian).
45. A.V. Nedolya and D.Y. Shapar, Estimation of energy of cubic iron-carbon nanoclusters by molecular mechanic method, *Materialwiss Werkst.*, **47**, Nos. 2–3: 128 (2016); https://doi.org/10.1002/mawe.201600481
46. A.V. Nedolya and N.V. Bondarenko, Change of energy of the cubic subnanocluster of iron under influence of interstitial and substitutional atoms, *Nanoscale Res. Lett.*, **11**: 15 (2016); https://doi.org/10.1186/s11671-016-1239-6
47. V.A. Andryuschenko and Ye.M. Dzevin, *Metallofiz. Noveishie Tekhnol.*, **19**, No. 3: 60 (1997) (in Russian).
48. A.V. Paustovskiy and Yu.V. Gubin, *Phys. Chem. Mech. Mater.*, No. 66: 31 (1997) (in Russian).
49. V.E. Danilchenko and B.B. Polchuk, *Fiz. Met. Metalloved.*, **91**, No. 5: 103, (2001) (in Russian).
50. V.E. Danilchenko and B.B. Polchuk, *Reports of the National Academy of Sciences of Ukraine*, No. 1: 137 (1998) (in Russian).
51. M.S. Kovalchenko, A.V.Paustovsky, and V.P. Botvinko, *Functional Materials*, No. 1: 135 (2001) (in Russian).
52. I. Schmidt and E. Hornbogen, The formation of metastable crystalline phases and glasses in splat-cooled Fe–C-Alloys, *Z. Metallkunde*, **69**, No. 4: 221 (1978); https://doi.org/10.1515/ijmr-1978-690404
53. Y.W. Kim, P.R. Strutt, and H. Nowotny, Laser melting and heat treatment of m2 tool steel: a microstructural characterization, *Metall. Mater. Trans. A*, **10**: 881 (1979); https://doi.org/10.1007/BF02658307
54. V.E. Danil'chenko, High-carbon martensite decomposition and formation of carbon-enriched regions, *Scripta Met.*, **23**, No. 11: 1823 (1989); https://doi.org/10.1016/0036-9748(89)90464-X
55. L.S. Palatnik, *Doklady Akademii Nauk SSSR*, **89**, No. 3: 455 (1953) (in Russian).
56. V.I. Lakomskiy and G.F. Torkhov, *Doklady Akademii Nauk SSSR*, **183**, No. 1: 87 (1968) (in Russian).
57. A.A. Uglov and A.L. Galiev, *Phys. Chem. Mater. Treat.*, No. 4: 10 (1981) (in Russian).
58. A.L. Galiev, L.L. Krapivin, and L.I. Mirkin, *Doklady Akademii Nauk SSSR*, **251**, No. 2: 336 (1980) (in Russian).
59. M.A. Krishtal, A.A. Zhukov, and A.N. Kokora, *Struktura i Svoistva Splavov, Obrabotannykh Izlucheniem Lasera* [Structure and Properties of Laser-Treated Alloys] (Moscow: Metallurgiya: 1973) (in Russian).
60. V.A. Tatarenko, T.M. Radchenko, and V.M. Nadutov, Parameters of interatomic interaction in a substitutional alloy f.c.c. Ni–Fe according to experimental data about the magnetic characteristics and equilibrium values of intensity of a diffuse scattering of radiations, *Metallofiz. Noveishie Tekhnol.*, **25**, No. 10: 1303 (2003) (in Ukrainian).

61. V.A. Tatarenko, S.M. Bokoch, V.M. Nadutov, T.M. Radchenko, and Y.B. Park, Semi-empirical parameterization of interatomic interactions and kinetics of the atomic ordering in Ni–Fe–C permalloys and elinvars, *Defect Diffus. Forum*, **280–281**: 29 (2008);
https://doi.org/10.4028/www.scientific.net/DDF.280-281.29
62. T.M. Radchenko and V.A. Tatarenko, Atomic-ordering kinetics and diffusivities in Ni–Fe permalloy, *Defect Diffus. Forum*, **273–276**: 525 (2008);
https://doi.org/10.4028/www.scientific.net/DDF.273-276.525
63. V.A. Tatarenko and T.M. Radchenko, The application of radiation diffuse scattering to the calculation of phase diagrams of f.c.c. substitutional alloys, *Intermetallics*, **11**, Nos. 11–12: 1319 (2003);
https://doi.org/10.1016/S0966-9795(03)00174-2
64. T.M. Radchenko, V.A. Tatarenko, and S.M. Bokoch, Diffusivities and kinetics of short-range and long-range orderings in Ni–Fe permalloys, *Metallofiz. Noveishie Tekhnol.*, **28**, No. 12: 1699 (2006).
65. T.M. Radchenko, O.S. Gatsenko, V.V. Lizunov, and V.A. Tatarenko, Martensitic α''-$Fe_{16}N_2$-type phase of non-stoichiometric composition: current status of research and microscopic statistical-thermodynamic model, *Prog. Phys. Met.*, **21**, No. 4: 580 (2020);
https://doi.org/10.15407/ufm.21.04.580
66. T.M. Radchenko, V.A. Tatarenko, H. Zapolsky, and D. Blavette, Statistical-thermodynamic description of the order–disorder transformation of $D0_{19}$-type phase in Ti–Al alloy, *J. Alloys Compd.*, **452**, No. 1: 122 (2008);
https://doi.org/10.1016/j.jallcom.2006.12.149
67. L. Cheng, A. Böttger, Th.H. de Keijser, and E.J. Mittemeijer, Lattice parameters of iron–carbon and iron–nitrogen martensites and austenites, *Scr. Metal. Mater.*, **24**, No. 3: 509 (1990);
https://doi.org/10.1016/0956-716X(90)90192-J
68. S.F. Yuriev, *Technical Physics*, **20**, No. 5: 47 (1950) (in Russian).
69. I.Z. Mogilevskiy, *Strukturnye Izmeneniya v Zheleze i Stali Posle Elektroiskrovoy Obrabotki Ikh Poverkhnosti Grafitom. Problemy Elektricheskoy Obrabotki Materialov* [Structural Changes in Iron and Steel After Electrospark Treatment of Their Surface with Graphite. Electrical Material Handling Challenges] (Moscow: Izdatelstvo AS USSR: 1984) (in Russian).
70. V.Yu. Danilchenko and O.M. Semyrga, Regularities of formation of carbide electrospark coatings on a steel substrate, *Superhard Materials*, No. 3: 57 (2005) (in Ukrainian).
71. A.M. Blokhin and I.G. Shveitser, *Rentgenospektralnyy Spravochnik* [X-Ray Spectral Handbook] (Moscow: Nauka: 1982) (in Russian).
72. I.E. Lev, V.V. Podkidyshev, and B.G. Lazarev, *Analiz Azotosoderzhashchikh Soedineniy v Splavakh Zheleza* [Analysis of Nitrogen-Containing Compounds in Iron Alloys] (Moscow: Metallurgiya: 1987) (in Russian).
73. V.A. Andryuschenko, Ye.M. Dzevin, and T.V. Yefimova, *Metallofiz. Noveishie Tekhnol.*, **20**, No. 7: 49 (1998) (in Russian).
74. V.A. Andryushchenko and E.N. Dzevin, *Bulletin of the Czech and Slovak Crystallographic Association*, **5**, Spec. Iss.: 20 (1999).
75. V.A. Andryuschenko, O.V. Bavol, T.L. Blinokhvatov, A.G. Garan, E.M. Dzevin, and G.S. Mogil'nyy, *Metallofiz. Noveishie Tekhnol.*, **31**, No. 9: 1257 (2009) (in Russian).

Received 20.01.2022;
in final version, 04.04.2022

В.Ю. Данільченко, Є.М. Дзевін, О.М. Семирга
Інститут металофізики ім. Г.В. Курдюмова НАН України,
бульв. Академіка Вернадського, 36,
03142 Київ, Україна

ФАЗОВІ ТА СТРУКТУРНІ ПЕРЕТВОРЕННЯ У СТОПАХ НА ОСНОВІ Fe ПІД ДІЄЮ КОМБІНОВАНОГО ВИСОКОЕНЕРГЕТИЧНОГО ОБРОБЛЕННЯ

Рентґенографічним, металографічним і мікродюрометричним методами досліджено та проаналізовано фазовий склад і структурно-напружений стан стопів на основі Fe під дією електроіскрового оброблення в комбінації з лазерним обробленням. Показано, що структурно-фазовий склад електроіскрового покриття на сталевій підкладинці визначається рядом чинників: дисоціацією карбіду WC на поверхні леґувального електрода на складові W_2C і W та подальшою ерозією їх, взаємодією продуктів ерозії з елементами міжелектродного середовища (C, N, O), взаємною дифузією елементів покриття та сталевої підкладинки, а також висхідною дифузією C із приповерхневих шарів підкладинки. Виявлено складний структурно-напружений стан гетерофазного покриття та приповерхневих шарів підкладинки; показано, що залишкові напруження у різних фазових складових формувалися за різними закономірностями: у сполуці на основі TiC формувалися розтягувальні напруження, а в складових W_2C, W, Fe_α — стискувальні напруження. Виявлено вибірковий вплив лазерного нагрівання покриття на напруження різного знаку.

Ключові слова: електроіскрове оброблення, лазерне оброблення, залишкові напруження, мартенситне перетворення, ерозія, дифузія, масоперенесення, карбід, нітрид.